

71. Nucleic-Acid Analogues with Restricted Conformational Flexibility in the Sugar-Phosphate Backbone ('Bicyclo-DNA')

Part 3¹⁾

Synthesis, Pairing Properties, and Calorimetric Determination of Duplex and Triplex Stability of Decanucleotides from [(3'S,5'R)-2'-Deoxy-3',5'-ethano- β -D-ribofuranosyl]adenine and -thymine

by Markus Tarköy²⁾, Martin Bolli²⁾, and Christian Leumann*

Institute of Organic Chemistry, University of Bern, Freiestrasse 3, CH-3012 Bern³⁾

In memoriam Jakob Schreiber

(22.II.94)

The synthesis of a new type of oligonucleotide ('bicyclooligodeoxynucleotide' = bcd(X_n)) displaying less conformational flexibility in its sugar-phosphate backbone is described, and a characterization of the pairing properties and energetics of the decamers bcd(T₁₀) and bcd(A₁₀) with each other and with complementary RNA and DNA sequences by UV-spectroscopic and calorimetric techniques is given. The results can be summarized as follows: *i*) bcd(T₁₀) pairs less strongly to complementary RNA and DNA, whereas bcd(A₁₀) forms stronger duplexes relative to the natural system. *ii*) bcd(A₁₀) discriminates between a complementary oligodeoxynucleotide with a mismatch in the center in the same way as d(A₁₀), indicating equal base-pairing selectivity. *iii*) bcd(A₁₀) forms more stable triplexes with d(T₁₀) of the pyrimidine-purine-pyrimidine (py · pu · py) motif than d(A₁₀). *iv*) The stability of duplexes containing a bicyclic strand is more sensitive towards salt concentration. The higher sensitivity in bcd(A₁₀) containing duplexes is due to a higher differential cation uptake. *v*) Differential scanning calorimetric (DSC) analysis of duplex-formation enthalpies shows ΔH^{FH} in all duplexes containing bicyclooligonucleotides to be more negative than ΔH^{cal} , which is compatible with the formation of catenated structures. *vi*) Isothermal titration calorimetry (ITC) provides a complete set of thermodynamic data including duplex and triplex association constants for the systems d(A₁₀)/d(T₁₀), bcd(A₁₀)/d(T₁₀), d(A₁₀)/bcd(T₁₀), bcd(A₁₀)/bcd(T₁₀). *vii*) All duplexes containing bicyclic strands show a (numerically) reduced pairing entropy term with respect to that of the natural system. *viii*) Enthalpies from DSC and ITC are similar, suggesting that the enthalpic contribution from ordered single strands to the overall duplex-formation enthalpy plays a minor role in the duplexes investigated.

1. Introduction. – Sequence-specific complexation of RNA single strands and duplex DNA by oligonucleotide analogues displaying strong and selective complex formation and high resistance against enzymatic degradation is of general interest in medicinal chemistry [4]. Such analogues may serve as selective inhibitors of protein biosynthesis. To investigate the potential of enhancing duplex (and triplex) stability entropically, by hybridizing an oligonucleotide analogue with a structurally less flexible sugar-phosphate

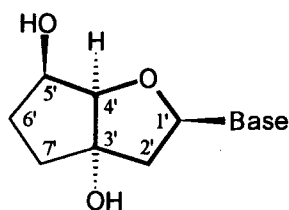
¹⁾ Part 2: [1].

²⁾ Taken in part from the Ph. D. Thesis of *M. T.* [2] and from the planned Ph. D. Thesis of *M. B.* [3].

³⁾ Part of the experiments described in this article were performed at the Laboratory of Organic Chemistry, ETH, Zürich.

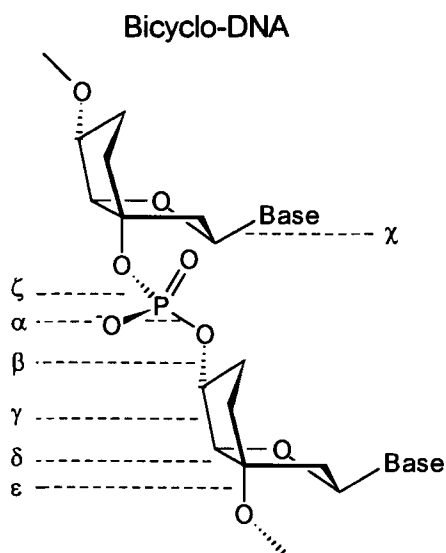
backbone to DNA or RNA complements, we recently designed and synthesized a new type of nucleoside ('bicyclodeoxynucleoside' = bcdX⁴) that differs from the natural deoxyribonucleosides by an additional ethylene bridge between the centers C(3') and C(5') (Fig. 1) [5]. The ethylene bridge in these nucleoside analogues primarily serves to restrict the rotational freedom around the C(3')–C(4') and the C(4')–C(5') bond, thereby affecting two (γ and δ) of the six torsional angles (Fig. 1) that describe the repeating nucleotide unit in DNA duplexes of the A and B type. The configuration at the centers C(3') and C(5') was chosen as to match the geometry of a natural nucleotide unit in duplex DNA (A or B) as close as possible.

Bicyclodeoxynucleosides



- 1 Base = Thy
- 2 Base = Ade
- 3 Base = Cyt
- 4 Base = Gua

Fig. 1. Bicyclodeoxynucleosides of the four natural bases and bicyclo-DNA with backbone torsion angles

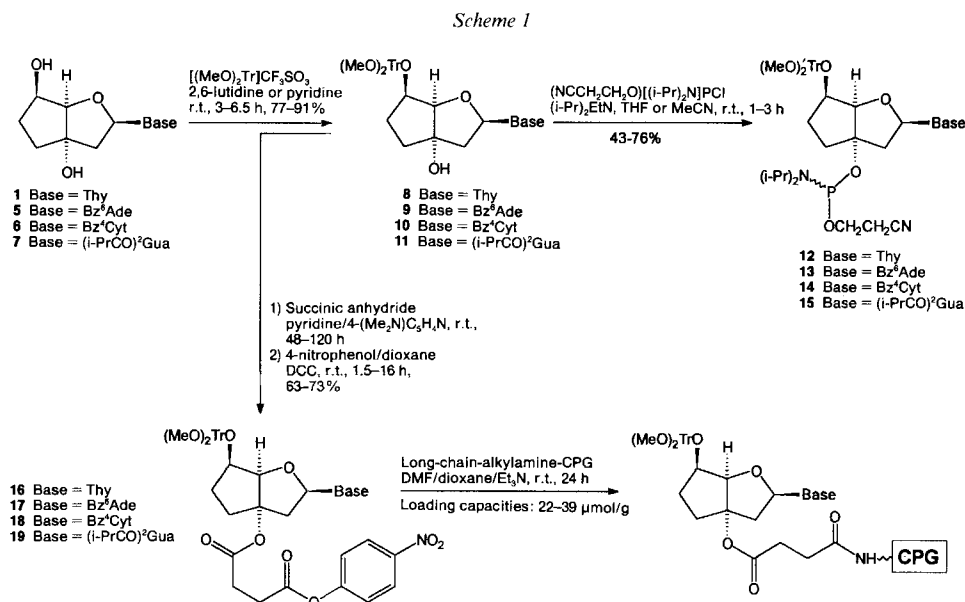


The expectation that the presence of a substituent at C(3') would restrict the furanose part of the bicyclonucleosides to an S-type conformation (2'-endo,1'-exo) was essentially confirmed in the solid state by X-ray analysis of the bicyclothymidine **1** (bcdT) [2] [5] and of the dinucleotide bcd(C₂) of bicyclodeoxycytidine [3] [6], and in solution by ¹H-NMR coupling-constant analysis of the latter and of the bicyclodeoxynucleosides **1–4**, respectively. Furthermore, variable-temperature NMR analysis of **1** gave no indication of the presence of other populated conformational states of the bicyclodeoxynucleosides. In all cases, the secondary OH group at C(5') appears uniformly in a pseudoequatorial position, while the orientation of the base substituent is preferentially 'anti' to the bicyclic ring system. While the intranucleoside torsion angles δ and χ in the bicyclodeoxynucleosides closely correspond to those of the repeating nucleotide unit in duplexes of the B form, the torsion angle γ prefers the anticlinal range with the OH substituent at C(5') in a

⁴) Following the IUPAC recommendations for the abbreviation of nonnatural nucleoside derivatives [12], we use the *ad hoc* lettering 'bcd' denoting a bicyclodeoxynucleoside residue. All other conventions are adapted in analogy to those for natural oligonucleotides. Duplexes are denoted with a dot between the sequence symbols (e.g. bcd(A₁₀)·d(T₁₀)), whereas stoichiometric mixtures differing from 1:1 are referred to by a slash (e.g. bcd(A₁₀)/d(T₁₀)).

pseudoequatorial position. This is found to deviate from that observed in natural duplex DNA, where γ adopts a synclinal orientation, corresponding to an axial orientation of the OH substituent in the bicyclic deoxynucleosides. In a recent communication [1], we demonstrated that decanucleotides of bicyclic deoxyadenosine **2** (bcdA) and bicyclic thymidine **1** effectively pair to their natural RNA and DNA complements exhibiting a higher propensity for triplex formation with DNA of the (py·pu·py) type relative to the natural system. In this communication, we describe the preparation of the phosphoramidite building blocks of all four bicyclic deoxynucleosides **1–4**, the automated solid-phase synthesis of oligonucleotides from **1** and **2**, and a detailed analysis of the thermodynamic data of duplex and triplex formation of the deca(bicyclic deoxynucleotides) bcd(A₁₀)⁴ and bcd(T₁₀)⁴ and their natural equivalents by differential scanning microcalorimetry (DSC) and isothermal titration calorimetry (ITC).

2. Oligo(bicyclic deoxynucleotides). – 2.1. *Building Blocks.* For the assembly of oligo-(bicyclic deoxynucleotides), we decided to adopt the phosphoramidite variant [7] of the phosphite-triester method [8] in nucleic-acid synthesis. This method is very versatile and was successfully applied in the past for the synthesis of a wide variety of nucleic-acid analogues [9]. A major point of concern was, whether this methodology would allow the efficient formation of secondary and tertiary phosphodiester bonds, as required by the nature of the bicyclic deoxynucleosides. The synthesis of the oligonucleotide building blocks **12–15** is depicted in *Scheme 1*.



The first goal was the synthesis of the 5'-O-protected nucleosides **8–11**, starting from the bicyclic deoxynucleosides **1** and **5–7** [5]. Attempts to prepare these intermediates by reaction with dimethoxytrityl chloride $[(\text{MeO})_2\text{Tr}]\text{Cl}$ according to standard procedures

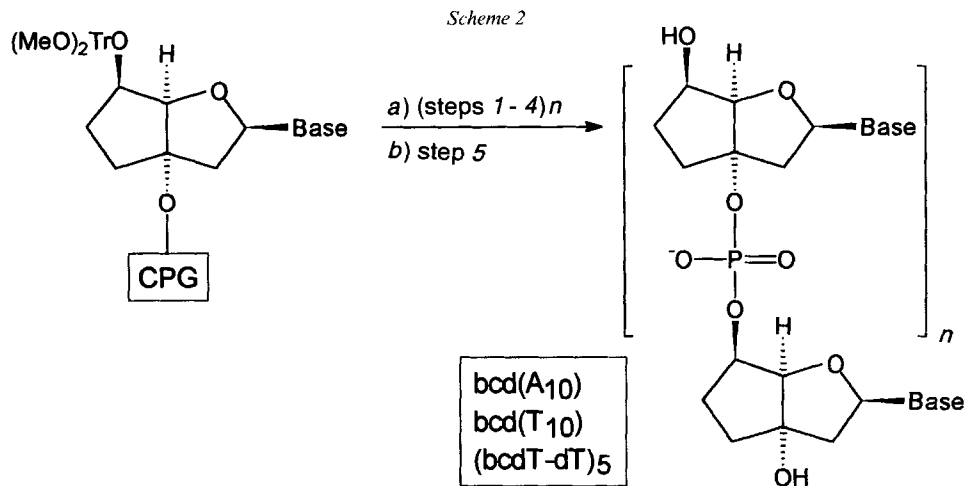
[10] failed. In all cases, virtually no reaction, even in the presence of perchlorate ions as a tritylation catalyst [11], was observed. As a more reactive agent, we investigated the corresponding triflate $[(\text{MeO})_2\text{Tr}]\text{CF}_3\text{SO}_3$, which was easily obtained in crystalline form by reaction of $[(\text{MeO})_2\text{Tr}]\text{Cl}$ with silver triflate in THF. Using this reagent, the desired conversion of **1** and **5–7** to the bicyclic deoxynucleoside derivatives **8–11** in 2,6-dimethylpyridine (= 2,6-lutidine) or pyridine as solvent took place in yields of 75–92%. As expected, no tritylation of the tertiary OH groups was observed. Subsequent elaboration of the phosphoramidite building blocks **12–15** was effected by reaction of the tritylated bicyclic deoxynucleosides **8–11** with chloro(2-cyanoethoxy)(diisopropylamino)phosphine in THF and proceeded in the same manner as in the case of the natural deoxynucleosides, irrespective of the different steric environment of the reacting center (secondary vs. tertiary OH group). The phosphoramidites **12–15**, thus obtained as mixtures of diastereoisomers (ca. 1:1 ratio as determined by ^1H - and ^{31}P -NMR), could easily be purified by conventional column chromatography and stored at -20° for months without observable decomposition. Nucleoside-modified solid support was prepared following standard protocols in nucleic-acid chemistry [10] by reaction of the nitrophenyl esters **16–19** with long-chain-alkylamine-CPG[®] (CPG = controlled-pore glass). Loading capacities of 22–39 μmol nucleoside/g CPG were obtained (trityl assay). Esters **16–19** were synthesized in yields of 63–73% by reaction of the tritylated precursors **8–11** with succinic anhydride and esterification of the corresponding succinates with 4-nitrophenol using dicyclohexylcarbodiimide (DCC) as the coupling reagent.

2.2. *Oligo(bicyclic deoxynucleotides)*. The synthesis of the oligo(bicyclic deoxynucleotides) $\text{bcd}(\text{A}_{10})$ and $\text{bcd}(\text{T}_{10})$ as well as of the chimaeric decamer $(\text{bcdT-dT})_5$ used in the present study was performed on a *Pharmacia-Gene-Assembler-Plus*[®] DNA synthesizer in scales of 0.6–10 μmol ⁵⁾. The synthesis cycle (*Scheme 2*) is completely compatible with that of the natural DNA synthesis. The only parameters changed were the detritylation and coupling time which were slightly extended relative to that for the synthesis of natural DNA oligomers [13]. Reagent and phosphoramidite concentrations as well as the phosphoramidite/*1H*-tetrazol ratio remained unchanged. With this protocol, coupling efficiencies of > 98% per step (trityl assay) were obtained. After the chain assembly was complete (trityl-off mode), detachment from the solid support and removal of the base and phosphate protecting groups was effected in a standard manner by treatment with conc. NH_3 solution at 55° for 10–16 h.

Crude oligomers were purified by HPLC on anion-exchange and/or reversed-phase columns to homogeneity in both systems. The HPLC traces of the crude reaction mixtures of $\text{bcd}(\text{A}_{10})$ and $\text{bcd}(\text{T}_{10})$ (*Fig. 2*) independently reflect the high coupling yields. Analysis of the purified oligomers was performed by matrix-assisted laser-desorption-ionization time-of-flight mass spectroscopy (MALDI-TOF-MS) using the recently reported optimized matrix for oligonucleotide analysis [14]⁶⁾. The spectra of the three decamers $\text{bcd}(\text{A}_{10})$, $\text{bcd}(\text{T}_{10})$, and $(\text{bcdT-dT})_5$ (*Fig. 3*) essentially show the peaks of the

⁵⁾ The synthesis of the natural oligo(deoxynucleotides), used as reference or as duplexation partners in the present study, was performed according to the manual of the DNA synthesizer [13] using commercially available phosphoramidite building blocks. Purification was effected by HPLC (see *Exper. Part*).

⁶⁾ We would like to thank Drs. *H. Moser* and *U. Pielers*, Central Research Laboratories, *Ciba-Geigy AG*, Basel, for the opportunity of having the MALDI-TOF-MS recorded on their instrument.



Step			0.6–1.3- μmol Scale	10- μmol Scale
<i>Chain assembly</i>	1) Detritylation	3% CHCl_2COOH in $\text{CHCl}_2\text{CHCl}_2$	60 s	200 s
	2) Coupling	0.1M phosphoramidite 0.5M 1 <i>H</i> -tetrazole in MeCN	11 equiv. 139 equiv. 6 min	4 equiv. 30 equiv. 9 min
	3) Capping	3% 4-(Me_2N) $\text{C}_3\text{H}_4\text{N}$, 10% Ac_2O , 15% 2,4,6-trimethyl- pyridine in MeCN	0.8 min	1.2 min
	4) Oxidation	0.01M I_2 in 2,4,6-trimethyl- pyridine/ H_2O / MeCN 1:6:11	18 s	1 min
<i>Deprotection/detachment</i>	5) Detritylation as 1), followed by conc. aq. NH_3 soln., 55°, 10–16 h			

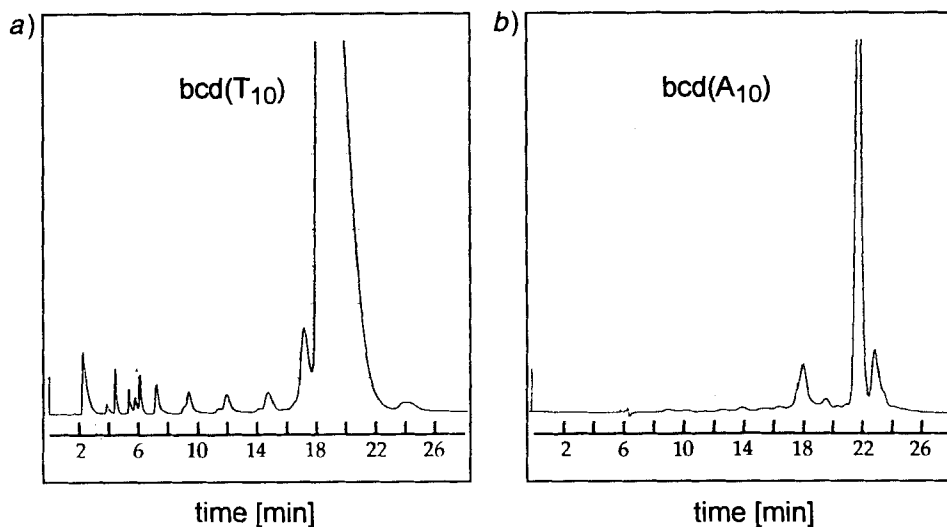


Fig. 2. HPLC Traces of crude synthesis products after deprotection. a) $\text{bcd}(\text{T}_{10})$ (reversed-phase chromatography); b) $\text{bcd}(\text{A}_{10})$ (DEAE chromatography). For details, see *Exper. Part*.

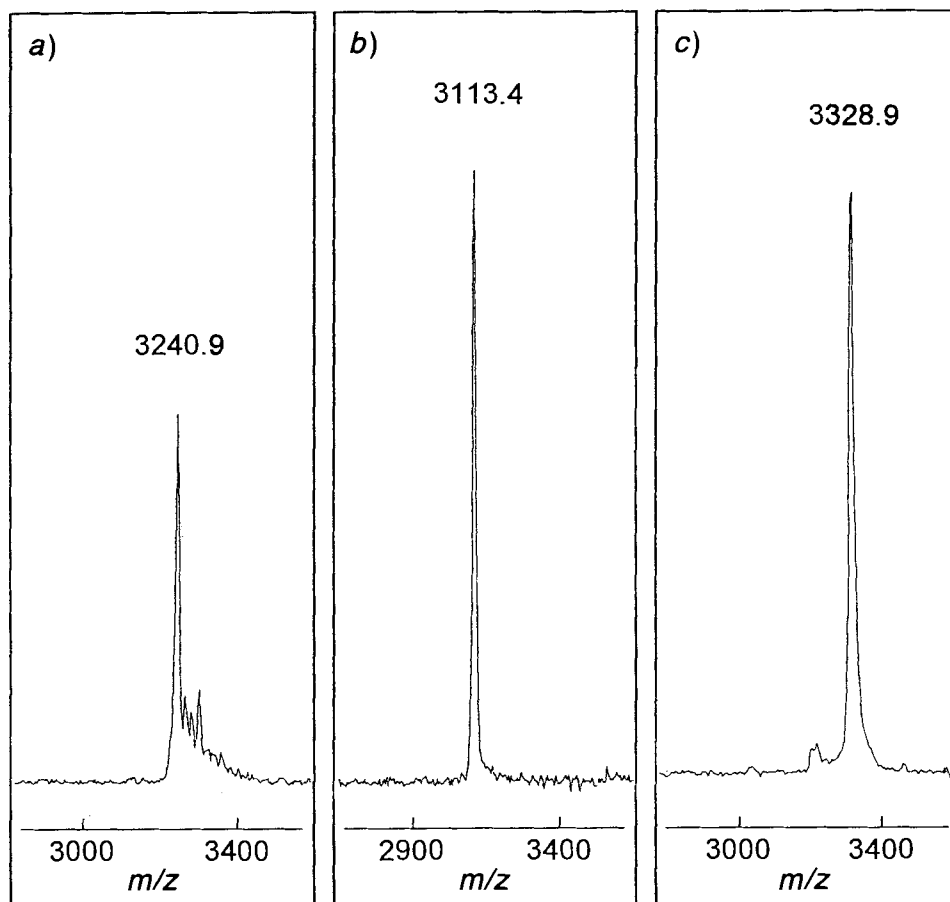


Fig. 3. MALDI-ToF-MS spectra of a) $bcd(T_{10})$, b) $(bcdT-dT)_5$, and c) $bcd(A_{10})$

molecular monoanions (remaining phosphodiester groups in form of their conjugated acid) at the expected molecular mass⁷⁾. Peaks at higher m/z can be assigned to sodium and/or potassium complexes of the corresponding molecular ions. Additionally, the oligomers $bcd(T_{10})$ and $bcd(A_{10})$ were enzymatically degraded by snake-venom phosphodiesterase/alkaline phosphatase and the products identified as the corresponding bicyclic deoxynucleosides **1** and **2** by HPLC (co-injection with authentic material) and by ¹H-NMR (in the case of $bcd(T_{10})$). Although having phosphodiester linkages to tertiary alkoxy groups, the oligo(bicyclic deoxynucleotides) are chemically stable, and no signs of degradation (HPLC control) under the conditions used for the investigation of their pairing properties (*e.g.* melting curves, calorimetric experiments) were observed.

⁷⁾ The difference between the experimentally determined mass (m/z) and the calculated molecular mass of the monoanions (-0.6 for $bcd(A_{10})$, $+1.5$ for $bcd(T_{10})$, and $+4.2$ for $(bcdT-dT)_5$) is above the tolerance of the instrument (0.5%) in the last case. Although we do not know the reason for this, the difference is too small to indicate a relevant alternative to the structure proposed.

3. Pairing Behavior of $bcd(A_{10})$ and $bcd(T_{10})$ to Complementary Sequences. – 3.1. *Self Structure and Pairing with Natural RNA Complements.* UV/Melting curves of pure $bcd(T_{10})$ and $bcd(A_{10})$ were recorded in neutral buffer containing 0.15M NaCl. For both, no cooperative transition in the temperature range 0–80° was observed (Fig. 4a). The max. hyperchromicities at 260 nm for $bcd(T_{10})$ (3%) and for $bcd(A_{10})$ (17%) indicate intra strand base stacking to be weak in the former, but pronounced in the latter case. Both

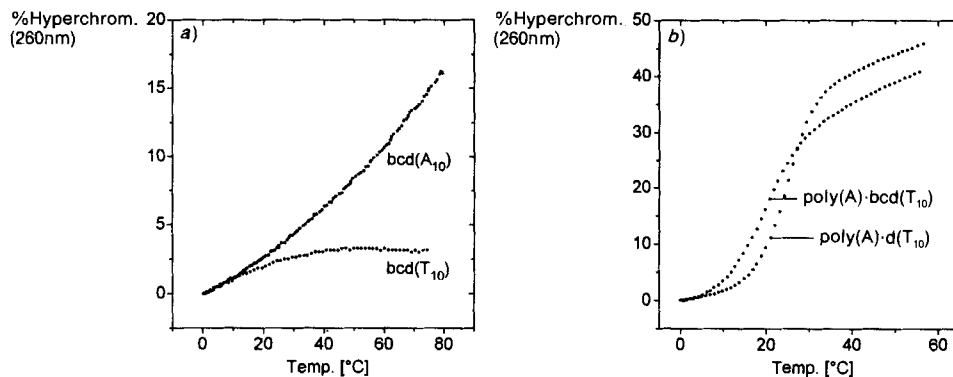


Fig. 4. UV/Melting curves of a) $bcd(T_{10})$ (10.8 μ M, 1M NaCl) and $bcd(A_{10})$ (4.8 μ M, 0.15M NaCl) and b) $poly(A) \cdot bcd(T_{10})$ and $poly(A) \cdot d(T_{10}) \cdot (c_{bp} = 50 \mu$ M, 0.15M NaCl) in 10 mM Tris \cdot HCl (pH 7.0)

Table 1. T_m Values and Hyperchromicities of Selected Duplexes and Triplexes Derived from UV/Melting Curves in 10 mM Tris \cdot HCl, pH 7.0

	A/T(U)-strand ratio (duplex or triplex conc.)	T_m (% hyperchromicity at 260 nm)	
		1M NaCl	0.15M NaCl
$bcd(A_{10})$ (4.8 μ M)			(15%)
$bcd(T_{10})$ (10.8 μ M)		(3%)	
$d(A_{10})/bcd(T_{10})^a$	1:1 (3.6 μ M)	27° (27%)	10° (20%)
	1:2 (3.6 μ M)	29° (23%)	13° (17%)
$bcd(A_{10})/d(T_{10})^a$	1:1 (3.7 μ M)	46° (37%)	25° (35%)
	1:2 (3.7 μ M)	47° (45%), 30° (10%)	28° (38%) ^{b)}
$d(A_{10})/d(T_{10})^a$	1:1 (3.2 μ M)	32° (32%)	24° (30%)
	1:2 (3.2 μ M)	34° (43%), 13° (14%)	25° (22%)
$bcd(A_{10})/bcd(T_{10})^a$	1:1 (3.3 μ M)	53° (47%)	35° (45%)
	1:2 (3.3 μ M)	55° (35%), 29° (7%)	36° (33%), ca. 5°
$bcd(A_{10})/poly(U)$	1:1 (26 μ M) ^{c)}		45° (50%)
$d(A_{10})/poly(U)$	1:1 (26 μ M) ^{c)}		32° (42%)
$poly(A)/bcd(T_{10})$	1:1 (48 μ M) ^{c)}	34° (40%)	20° (37%)
$poly(A)/d(T_{10})$	1:1 (46 μ M) ^{c)}	36° (40%)	24° (40%)
	1:2 (37 μ M) ^{c)}	43° (38%) ^{b)}	
$poly(dA)/bcd(T_{10})$	1:1 (45 μ M) ^{c)}	35° (37%)	7° (30%)
	1:2 (39 μ M) ^{c)}	33° (30%) ^{b)}	
$poly(dA)/d(T_{10})$	1:1 (46 μ M) ^{c)}	40° (50%)	27° (42%)
	1:2 (37 μ M) ^{c)}	43° (38%) ^{b)}	
$poly(dA)/(bcdT-dT)_5$	1:1 (47 μ M) ^{c)}	40° (50%)	25° (38%)
$d(A_{10})/(bcdT-dT)_5$	1:1 (4.2 μ M)	30° (35%)	21° (30%)

^{a)} Buffer: 10 mM NaH_2PO_4 , pH 7.0. ^{b)} Determination of T_m values not possible. ^{c)} Base-pair concentration.

bicyclo-DNA oligomers, therefore, seem to behave as their natural equivalents and show no signs of self-pairing. Complementary base pairing of $\text{bcd}(\text{T}_{10})$ with poly(A), however, occurs readily as monitored by its cooperative and reversible melting curve (Fig. 4b). This duplex is slightly less stable than that of $\text{d}(\text{T}_{10})$ with poly(A) ($\Delta T_m = -4^\circ$, 0.15M NaCl, Table 1). Under comparable conditions, $\text{bcd}(\text{A}_{10})$ pairs considerably stronger to poly(U) than does its natural equivalent $\text{d}(\text{A}_{10})$ ($\Delta T_m = +13^\circ$, 0.15M NaCl) [1]. Table 1 summarizes T_m values and hyperchromicities for all pairing systems investigated as derived from UV/melting curves.

UV/Mixing curves according to the method of Job [15] in the $\text{d}(\text{A}_{10})/\text{poly}(\text{U})^a$ system (0.15M NaCl, pH 7.0, 4°) at wavelengths between 250 and 285 nm show only single discontinuity at 66 mol-% U, whereas in the $\text{bcd}(\text{A}_{10})/\text{poly}(\text{U})$ system, double discontinuity is observed at 280 nm at 49 and 68 mol-% U (Fig. 5). While in the former case, the triplex is more stable than the duplex, irrespective of the base stoichiometry and buffer composition⁸), in the latter case, both duplex and triplex are formed at the appropriate stoichiometric ratios. Melting curves of a 1:1 mixture of poly(U) and $\text{d}(\text{A}_{10})$, therefore, are associated with a triplex \rightarrow single-strand dissociation, and that of poly(U) and $\text{bcd}(\text{A}_{10})$ with duplex rupture.

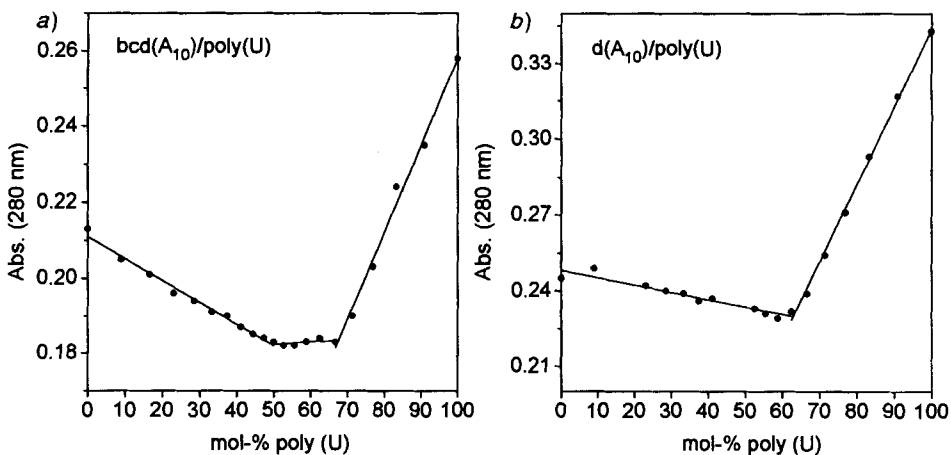


Fig. 5. UV/Mixing curves: a) $\text{bcd}(\text{A}_{10})/\text{poly}(\text{U})$ ($c_{\text{tot. base}} = 74 \mu\text{M}$) and b) $\text{d}(\text{A}_{10})/\text{poly}(\text{U})$ ($c_{\text{tot. base}} = 84 \mu\text{M}$) in 10 mM Tris·HCl/0.15M NaCl (pH 7.0)

The structures of the hybrid complexes under discussion were investigated by CD spectroscopy. From Fig. 6a it is evident that the hybrid duplexes $\text{poly}(\text{A}) \cdot \text{d}(\text{T}_{10})$, and $\text{poly}(\text{A}) \cdot \text{bcd}(\text{T}_{10})$ show almost identical CD curves indicating an analogous constitution and conformation of the two duplexes. The CD spectra of complexes of poly(U) with $\text{bcd}(\text{A}_{10})$ and with $\text{d}(\text{A}_{10})$ deviate from each other by a more intense positive Cotton effect at 263 nm in the bicyclic relative to the natural hybrid (Fig. 6b). Whether this is due to the

⁸) It was shown previously that $\text{poly}(\text{dA}) \cdot \text{poly}(\text{U})$ exists in neutral solution exclusively as the corresponding $\text{poly}(\text{dA}) \cdot 2 \text{poly}(\text{U})$ triplex irrespective of the base/base ratio and salt concentration [16].

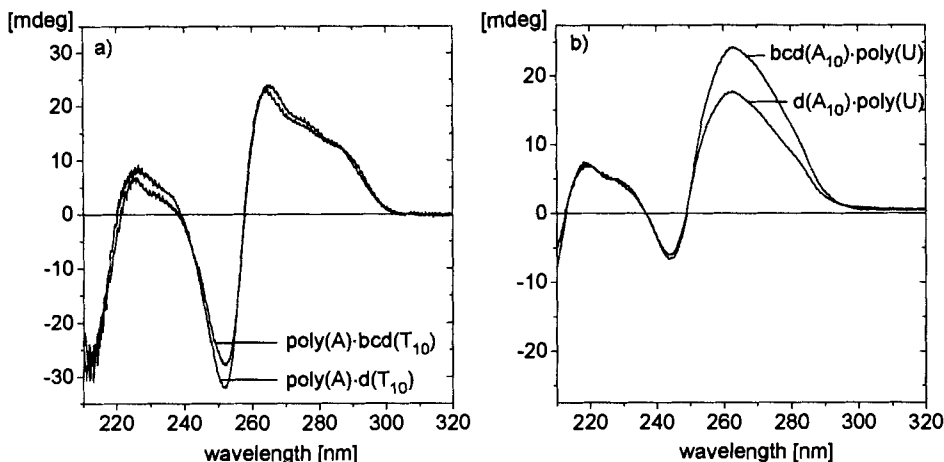


Fig. 6. CD spectra of a) $\text{poly(A)} \cdot \text{bcd}(T_{10})$ ($c_{\text{bp}} = 31 \mu\text{M}$, 2° , 1M NaCl) and $\text{poly(A)} \cdot \text{d}(T_{10})$ ($c_{\text{bp}} = 33 \mu\text{M}$, 2° , 1M NaCl) and b) $\text{bcd}(A_{10}) \cdot \text{poly(U)}$ ($c_{\text{bp}} = 34 \mu\text{M}$, 5° , 0.15M NaCl) and $\text{d}(A_{10}) \cdot \text{poly(U)}$ ($c_{\text{bp}} = 31 \mu\text{M}$, 0° , 0.15M NaCl) in $10\text{ mM Tris} \cdot \text{HCl}$ (pH 7.0)

difference in molecularity of the two complexes (triplex in the case of $\text{d}(A_{10}) \cdot \text{poly(U)}$ vs. duplex for $\text{bcd}(A_{10}) \cdot \text{poly(U)}$) or to other structural alterations remains open at this point. Taking into account that the bicyclocleoxynucleosides are structurally restricted to the S-type conformation (1'-*exo*, 2'-*endo*) in the furanose part [5] [6], oligomers thereof are expected to be restricted to a B-type sugar-phosphate backbone in the duplex. The similarity of the CD spectra, especially in the case of $\text{poly(A)} \cdot \text{bcd}(T_{10})$ and $\text{poly(A)} \cdot \text{d}(T_{10})$, therefore, supports the view, that natural DNA/RNA complexes can exist in heteronomous conformations with different sugar pucker in the constituent single strands in solution. Such heteronomous nucleic-acid structures were reported earlier for the duplexes $\text{poly(A)} \cdot \text{poly(dT)}$ by X-ray fiber diffraction [17a] and Raman spectroscopy [17b], for $\text{poly(dA)} \cdot \text{poly(U)}$ by fiber diffraction [18a] and CD spectroscopy [18b], as well as for oligo-DNA/RNA duplexes of mixed sequence [19], and for DNA triplexes [20] by NMR spectroscopy. The recent finding that mixed RNA/DNA triplex stability in the (py·pu·py) motif is largely dependent upon the backbone constitution (ribo- vs. deoxyribo-) of the constituent single strands was also interpreted in terms of non-canonical triplex conformations [21].

3.2. Pairing of $\text{d}(A_{10})$ with $\text{bcd}(T_{10})$ and $\text{d}(T_{10})$ and of $\text{bcd}(A_{10})$ with $\text{d}(T_{10})$ and $\text{bcd}(T_{10})$. Melting curves of mixtures of $\text{d}(A_{10})/\text{bcd}(T_{10})$, $\text{bcd}(A_{10})/\text{d}(T_{10})$, $\text{bcd}(A_{10})/\text{bcd}(T_{10})$, and $\text{d}(A_{10})/\text{d}(T_{10})$ in stoichiometric ratios 'A/T' 1:1 and 1:2 were recorded at comparable oligonucleotide concentrations in neutral buffer containing 0.15M and 1M NaCl , respectively (Fig. 7). At the molar ratio 'A/T' 1:1, all systems exhibit monophasic reversible sigmoidal melting curves at both (0.15 and 1M) salt concentrations, indicative for cooperative melting of duplex structures. Duplexes containing $\text{bcd}(A_{10})$ exhibit higher hyperchromicity (10–15%) and those containing $\text{bcd}(T_{10})$ an almost equal value relative to the natural system at comparable wavelengths (Table 1). From the T_m values, it is evident that under low salt conditions (0.15M NaCl), $\text{bcd}(T_{10})$ binds less strongly to $\text{d}(A_{10})$ than its natural equivalent ($\Delta T_m(\text{duplex}) = -13^\circ$), whereas $\text{bcd}(A_{10})$ binds essentially

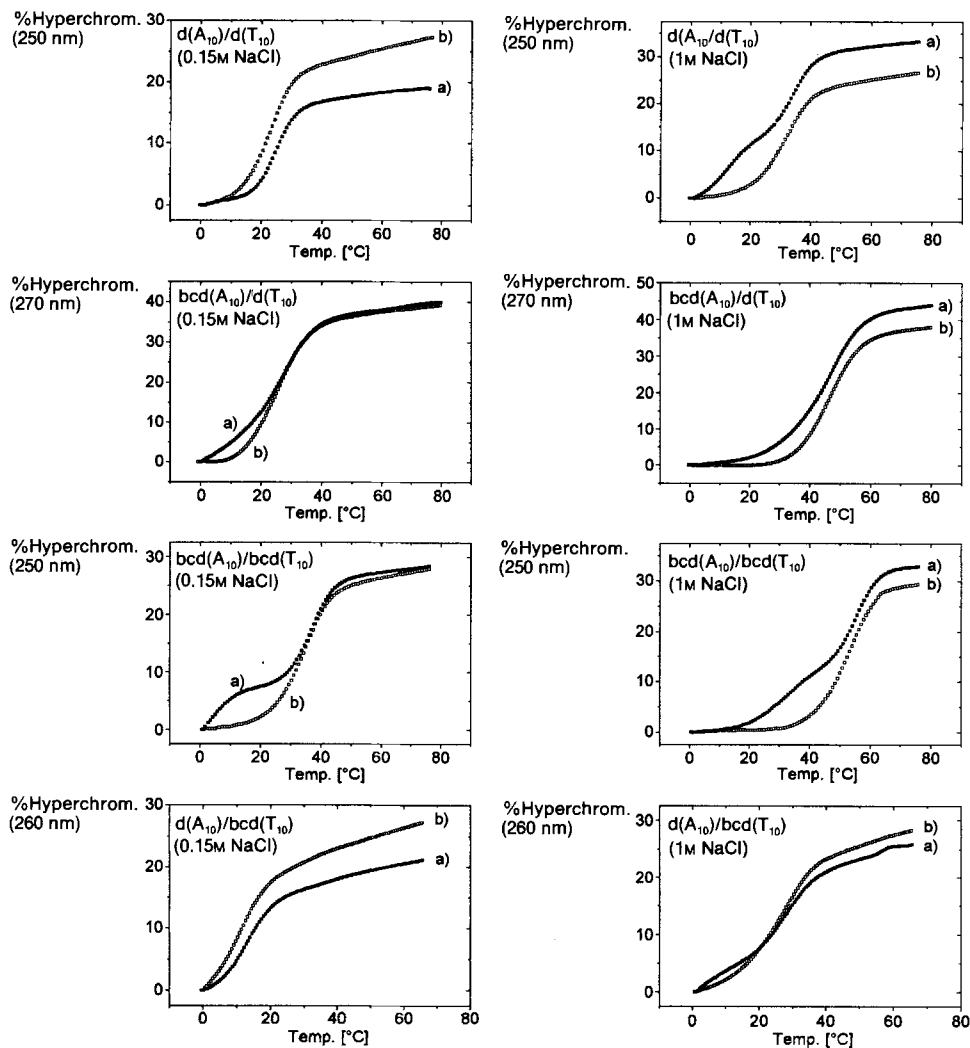


Fig. 7. UV/Melting curves of stoichiometric mixtures 'A/T' 1:2 (curves a) and 'A/T' 1:1 (curves b) in 10 mM NaH_2PO_4 (pH 7.0) containing 0.15M or 1M NaCl ($c = 3.6\text{--}3.9 \mu\text{M}$)

equally well to $d(T_{10})$ than $d(A_{10})$ ($\Delta T_m(\text{duplex}) = +2^\circ$). In this permutational series, the completely bicyclic system $\text{bcd}(A_{10})/\text{bcd}(T_{10})$ forms the strongest duplex with $\Delta T_m = +10^\circ$ relative to its natural equivalent.

At the molar ratio 'A/T' 1:2 and high (1M) salt concentration (Fig. 7, Table 1), all systems show biphasic, cooperative, and reversible melting curves⁹⁾. The transition at high temperature is in the same range as that of the 1:1 complexes and associated with

⁹⁾ The melting process at low temperature is also completely reversible at the temperature scan rate applied (0.5°/min), indicating that triplex equilibrium binding is observed.

duplex \rightarrow single-strand disruption. Consequently, the melting step at lower temperature corresponds to the triplex \rightarrow duplex transition¹⁰). At low salt concentration (0.15M NaCl), triplex formation can already be observed in the case of $\text{bcd}(\text{A}_{10})/\text{d}(\text{T}_{10})$ and $\text{bcd}(\text{A}_{10})/\text{bcd}(\text{T}_{10})$, but not in the natural $\text{d}(\text{A}_{10})/\text{d}(\text{T}_{10})$ and in the hybrid $\text{d}(\text{A}_{10})/\text{bcd}(\text{T}_{10})$. The melting curve of the 1:2 mixture of $\text{bcd}(\text{A}_{10})/\text{d}(\text{T}_{10})$ at low and high salt concentration (Fig. 7) can be deconvoluted as two highly overlapping melting processes with T_m values of the triplex \rightarrow duplex and the duplex \rightarrow single-strand transitions to be near to each other. The possibility of a monophasic triplex \rightarrow single strand melting can be excluded by means of the UV/mixing curve [1] which shows two intersection points at molar 'A/T' ratios of 33 and 50%, respectively, and by means of titration calorimetry (*vide infra*). T_m Values for triplex \rightarrow duplex transitions are listed in Table 1. From these data, it is evident that triplex formation in complexes containing the bicyclic purine strand is favored over triplex formation in the natural system and in the $\text{d}(\text{A}_{10})/\text{bcd}(\text{T}_{10})$ hybrid. Furthermore, mixing curves of $\text{d}(\text{A}_{10})/\text{bcd}(\text{T}_{10})$, and $\text{bcd}(\text{A}_{10})/\text{bcd}(\text{T}_{10})$ (Fig. 8) indicate no triplex formation at the stoichiometric ratio 'A/T' 2:1, ruling out the possibility of an alternative (pu·pu·py)-like triplex formation between two purine and one pyrimidine strand.

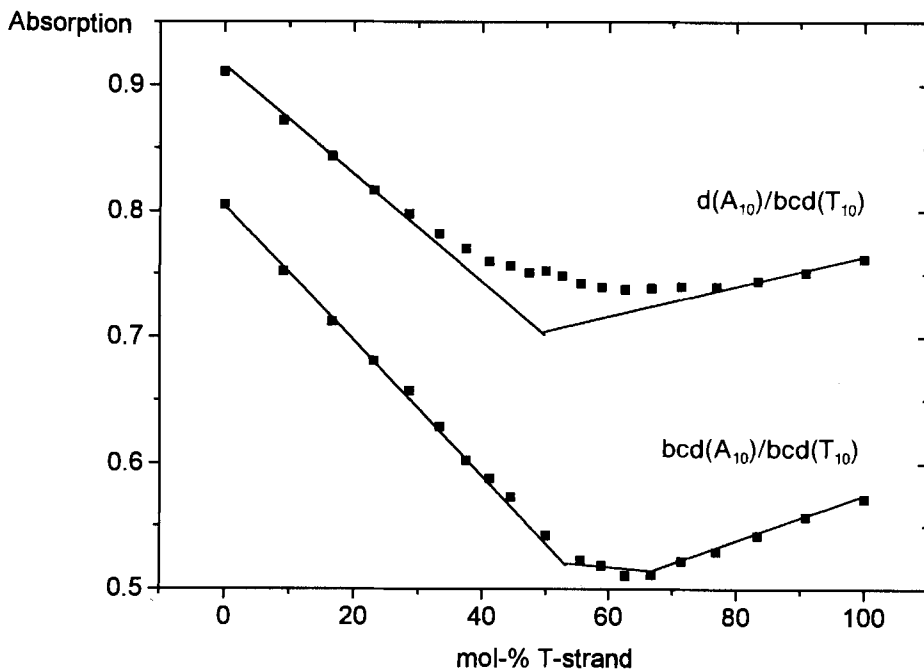


Fig. 8. UV/Mixing curves of $\text{d}(\text{A}_{10})/\text{bcd}(\text{T}_{10})$ ($c_{\text{tot}} = 8.9 \mu\text{M}$, 0.15M NaCl, 8°, 260 nm) and $\text{bcd}(\text{A}_{10})/\text{bcd}(\text{T}_{10})$ ($c_{\text{tot}} = 7.8 \mu\text{M}$, 10 mM MgCl_2 , 8°, 255 nm) in 10 mM Tris·HCl (pH 7.0)

¹⁰) In the natural series, the duplex \rightarrow single-strand transition is characterized by an isosbestic point at 284 nm in their UV spectra, whereas the triplex \rightarrow duplex transition is hyperchromic at that wavelength [16] [22]. In the bicyclic hybrid duplexes $\text{bcd}(\text{A}_{10}) \cdot \text{d}(\text{T}_{10})$ and $\text{bcd}(\text{A}_{10}) \cdot \text{bcd}(\text{T}_{10})$, no such isosbestic point is observed between 260 and 290 nm. Only duplex rupture in the case of $\text{d}(\text{A}_{10}) \cdot \text{bcd}(\text{T}_{10})$ is associated with an isosbestic point at 280 nm.

The mixing curve of $d(A_{10})/bcd(T_{10})$ deviates from the ideal straight lines near to equivalent strand concentrations (50 mol-%T) due to partial duplex melting under the experimental conditions applied (0.15M NaCl, 8°).

The CD spectra of $d(A_{10}) \cdot bcd(T_{10})$ and $bcd(A_{10}) \cdot d(T_{10})$ at 4 and 1°, respectively, are very similar to that of natural $d(A_{10}) \cdot d(T_{10})$ [22] at 7°, which is indicative of comparable duplex constitution (antiparallel strand orientation) and conformation (B-type) for the two bicyclic hybrids (Fig. 9). However, at 15°, the spectrum of $bcd(A_{10}) \cdot d(T_{10})$ shows a strongly enhanced positive Cotton effect at 259 nm and thus differs substantially from that of $d(A_{10}) \cdot d(T_{10})$ at the same temperature. Since this temperature is well below the melting temperature of both duplexes, the change indicates a structural ‘premelting’ event within the duplex structure of $bcd(A_{10}) \cdot d(T_{10})$ that is unique to this duplex. The elucidation

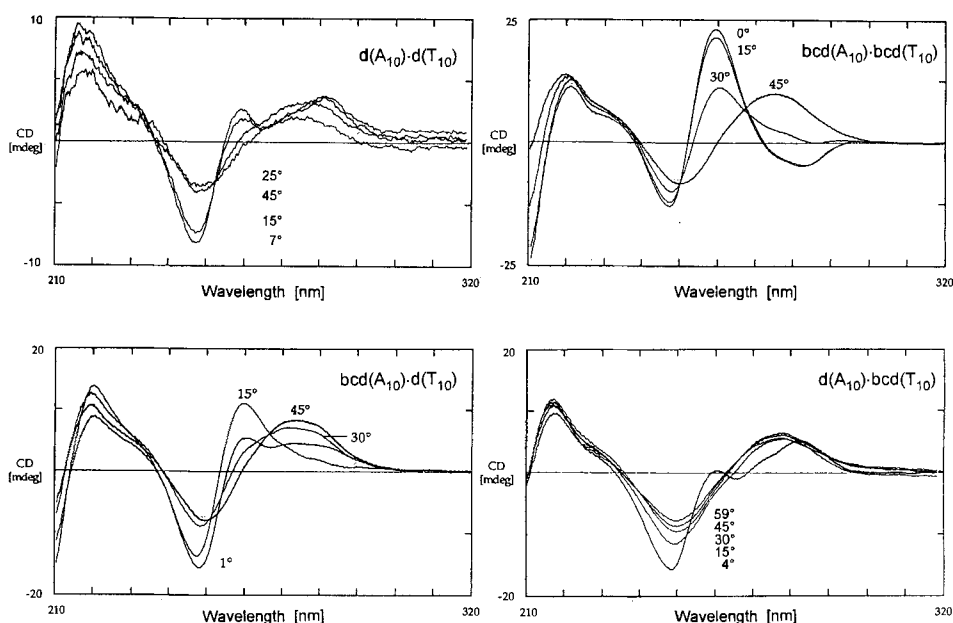


Fig. 9. CD Spectra of $d(A_{10}) \cdot d(T_{10})$ ($c = 6.2 \mu\text{M}$), $bcd(A_{10}) \cdot d(T_{10})$ ($c = 2.8 \mu\text{M}$), $bcd(A_{10}) \cdot bcd(T_{10})$ ($c = 2.8 \mu\text{M}$), and $d(A_{10}) \cdot bcd(T_{10})$ ($c = 5.0 \mu\text{M}$) in 10 mM Tris·HCl/0.15M NaCl (pH 7.0)

tion of the structural consequences of this premelting event, which is not observable in the corresponding UV/melting curves (Fig. 7), needs further investigations. The CD spectrum of the all-bicyclic decamer duplex $bcd(A_{10}) \cdot bcd(T_{10})$ differs considerably from those of natural DNA or RNA in the A-, B-, or Z-conformation, in that it shows a large positive Cotton effect at 259 nm and a new, negative band with minimum ellipticity at 282 nm in its non-denaturated state. In view of the relatively high stability of this duplex, the determination of its structural details is of considerable interest and is currently under way in our laboratory.

3.3. Pairing Selectivity. We addressed the question of base-pairing selectivity with a natural DNA complement by determining T_m values of duplexes of $bcd(A_{10})$ with the

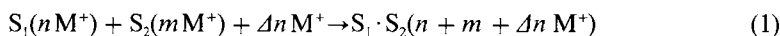
Table 2. ΔT_m Values from UV/Melting Curves (260 nm) of Mismatched Relative to Matched Duplexes
($c = 3.1 \mu\text{M}$ in 10 mM Tris · HCl/0.15M NaCl, pH 7.0)

ΔT_m	(5'-3')-d(T-T-T-T-T-X-T-T-T-T)			
	X			
	T	A	C	G
bcd(A ₁₀)	0	-20.1	-18.1	-18.6
d(A ₁₀)	0	-19.9	-18.8	-17.7

mismatch sequences d(T₅-X-T₄), where X represents one of the three remaining natural deoxynucleosides dA, dG, and dC (Table 2). For comparison, the same experiments were also performed in the natural series d(A₁₀) · d(T₅-X-T₄). As can be seen from the corresponding ΔT_m values, the discrimination of a sequence with one mismatch at the center occurs in both series to almost equal extent, showing the A · A mismatch ($\Delta T_m \approx 20^\circ$) being most destabilizing in both, followed by A · G and A · C in the mixed, and in reversed order in the natural mismatched duplex.

To check whether an additive, unfavorable pairing geometry in bcd(T₁₀) may be responsible for the poor binding of bcd(T₁₀) to d(A₁₀), we synthesized the alternating chimaeric decamer (bcdT-dT)₅, reasoning that interrupts in the bicyclic backbone by the structurally more flexible natural thymidine could partially compensate for strain present in the d(A₁₀) · bcd(T₁₀) duplex. In this case, one would expect the ΔT_m values per modification ($\Delta T_m/\text{mod.}$), relative to natural d(A₁₀) · d(T₁₀), to be smaller in the chimaeric d(A₁₀) · (bcdT-dT)₅ duplex than in d(A₁₀) · bcd(T₁₀). This is indeed the case, as can be seen from Table 1, where a $\Delta T_m/\text{mod.}$ of only -0.6° for the former vs. -1.3° for the latter duplex can be calculated.

4. Thermodynamic Properties. – 4.1. *Salt-Concentration Dependence of Duplex Formation.* Due to the polyanionic nature of DNA, duplex formation is strongly influenced by the presence of salt. Increasing salt concentration favors duplexation. Mainly two phenomena are responsible for this behavior [23] [24]: the shielding of the negative (repulsive) *Coulomb* charges and the differential binding of positive counter ions (Δn) to the duplex as expressed in Eqn. 1 where S₁, S₂, and S₁ · S₂ denote the two single strands and the duplex, respectively, and M⁺ a monovalent cation.



At NaCl concentrations below 1M, this second effect, entropic in nature, is dominating in nucleic-acid association. We investigated the dependence of the melting temperature from the NaCl concentration in all four duplexes and found, as expected, a linear relationship between T_m and $\ln [\text{NaCl}]$ (Fig. 10). In all cases where bicyclic oligodeoxynucleotides are involved in duplexation, we observe a stronger dependence of the T_m from the salt concentration which is expressed by the steeper slopes of the corresponding straight lines (Table 3). Salt sensitivity increases in the order d(A₁₀) · d(T₁₀) < d(A₁₀) · bcd(T₁₀) < bcd(A₁₀) · bcd(T₁₀) < bcd(A₁₀) · d(T₁₀). Bicyclo-DNA duplex formation could be associated with a higher differential cation uptake (larger Δn) relative to natural duplex formation as a direct (phosphate complexation) or indirect (different constitution or conformation of duplex or single strands, resp.) consequence of the ethylene bridge located in between the phosphodiester groups. The higher dependence of

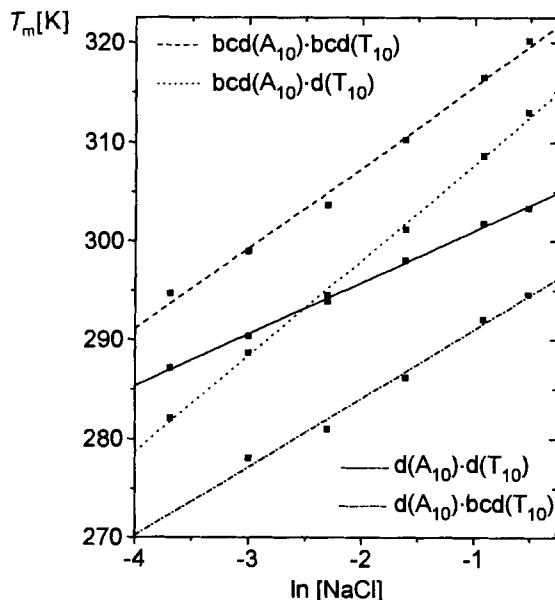


Fig. 10. T_m vs. $\ln [\text{NaCl}]$ plots of the four duplexes indicated ($c = 3.9 \mu\text{M}$ in $10 \text{ mM NaH}_2\text{PO}_4$, pH 7.0)

Table 3. Salt Dependence and Counter-Ion Uptake for Duplex Formation ($10 \text{ mM NaH}_2\text{PO}_4$, pH 7.0)

	$d(\text{A}_{10}) \cdot d(\text{T}_{10})$	$\text{bcd}(\text{A}_{10}) \cdot d(\text{T}_{10})$	$d(\text{A}_{10}) \cdot \text{bcd}(\text{T}_{10})$	$\text{bcd}(\text{A}_{10}) \cdot \text{bcd}(\text{T}_{10})$
$\partial T_m / \partial \ln [\text{NaCl}]$	5.24 ± 0.12	9.67 ± 0.21	6.93 ± 0.45	8.15 ± 0.33
Δn	3.64	5.07	3.15	4.43

T_m from salt concentration could also be due to the observed less negative overall pairing enthalpy and entropy compared with the natural system, indicating that the relative contribution of electrostatics with respect to stacking and H-bonding interactions to the overall pairing energy may be more pronounced in bicyclo-DNA compared to natural DNA. To examine the contribution of differential cation uptake, we calculated Δn (Table 3) for all four duplexes according to the polyelectrolyte theory [24] (Eqn. 2) using the transition enthalpies from the DSC experiments (Table 4).

$$\Delta n = -\frac{\partial T_m}{\partial \ln [\text{NaCl}]} \cdot \frac{2\Delta H_{\text{cal}}^0}{RT_m^2} \quad (2)$$

Table 4. Thermodynamic Data from DSC Experiments

	$d(\text{A}_{10}) \cdot d(\text{T}_{10})$	$d(\text{A}_{10}) \cdot \text{bcd}(\text{T}_{10})$	$\text{bcd}(\text{A}_{10}) \cdot d(\text{T}_{10})$	$\text{bcd}(\text{A}_{10}) \cdot \text{bcd}(\text{T}_{10})$
T_m [°C] (conc.)	45.3 (0.150 mM)	41.1 (0.141 mM)	62.5 (0.133 mM)	64.4 (0.100 mM)
ΔH^{DSC} [kcal · mol ⁻¹]	-70.0 ± 0.9	-44.7 ± 1.3	-58.7 ± 1.5	-61.5 ± 1.5
ΔH^{vH} [kcal · mol ⁻¹]	-61.8 ± 2.0	-51.3 ± 2.4	-64.0 ± 2.1	-74.6 ± 2.8
ΔS^{DSC} [cal · mol ⁻¹ · K ⁻¹]	-221 ± 3	-142 ± 4	-175 ± 4	-182 ± 3

The results indicate higher differential cation uptake in systems containing the bicyclic purine strand. This can be rationalized by duplex structures having more condensed negative charges relative to the single strands. If one makes the assumption that the phosphate-phosphate distances are, because of equal distance of the base pairs, similar in the natural and the hybrid duplexes, then the higher cation uptake would merely be the consequence of a more extended structure of the bicyclic oligonucleotide single strands. This seems not to be true for the duplex $d(A_{10}) \cdot bcd(T_{10})$ which displays a slightly smaller uptake of cations. The higher sensitivity of duplex stability towards salt concentration of this weakly pairing duplex could, therefore, be the consequence of a higher weight of the electrostatic contributions to overall duplex stability.

4.2. *Calorimetric Analysis of Duplex and Triplex Formation.* In our recent communication [1], we reported thermodynamic data of duplex formation obtained from UV/melting curves. This indirect method for deriving pairing enthalpies and entropies, however, is dependent upon models for the duplex-disruption mechanism. Although these models are fairly accurate for describing duplex \rightarrow single-strand transitions in natural oligonucleotides, it is not clear in advance, whether structural alterations, as in the case of bicyclo-DNA, could render such mechanistic assumptions, and concomitantly the derived thermodynamic data, obsolete. We, therefore, analyzed both duplex- and triplex-formation enthalpies and entropies for all deca(deoxynucleotides) by model-independent calorimetric methods.

4.2.1. *Differential Scanning Calorimetry.* Differential scanning calorimetry (DSC) was widely used for the determination of thermodynamic data for oligonucleotide-duplex [25] and -triplex [26] formation. We measured DSC curves (*Fig. 11*) for the four duplexes $d(A_{10}) \cdot d(T_{10})$, $bcd(A_{10}) \cdot d(T_{10})$, $d(A_{10}) \cdot bcd(T_{10})$, and $bcd(A_{10}) \cdot bcd(T_{10})$, in neutral buffer containing 1M NaCl on a *MicroCal-MC-2* differential-scanning microcalorimeter. Since, in a DSC curve, ΔC_p vs. T is recorded, pairing enthalpies ΔH^{DSC} were obtained by direct peak integration of the DSC curve (*Eqn. 3*) and entropies ΔS^{DSC} by dividing the heat signal by T followed by peak integration (*Eqn. 4*). Alternatively, *van't-Hoff* transition enthalpies (ΔH^{vH}), assuming a bimolecular two-state model for duplex disruption, were obtained by shape analysis of the DSC curves.

$$\int \Delta C_p \cdot dT = \Delta H^{DSC} \quad (3)$$

$$\int \frac{\Delta C_p}{T} \cdot dT = \Delta S^{DSC} \quad (4)$$

From these curves, it becomes evident that with the exception of $bcd(A_{10}) \cdot d(T_{10})$, there is no change in C_p before and after the melting event. Duplex melting of this system is accompanied by a ΔC_p of ca. 1.1 kcal/mol. This ΔC_p could be related to the structural 'premelting', unique to this duplex, observed by CD spectroscopy (*vide supra*). Enthalpy changes obtained by integration of the DSC curves (ΔH^{DSC}) show considerable differences to those obtained by the two-state-model-dependent shape analysis of the calorimetric curves (ΔH^{vH}). Since, in a multistate melting mechanism, a broader transition (and, therefore, a less negative ΔH^{vH} with respect to ΔH^{DSC}) is expected, differences in this direction are generally interpreted in terms of a deviation of the true melting mechanism from the bimolecular two-state model [25b]. This is indeed the case in the natural duplex $d(A_{10}) \cdot d(T_{10})$ where ΔH^{vH} is by 8.2 kcal/mol less negative, indicating that only ca. 88% of

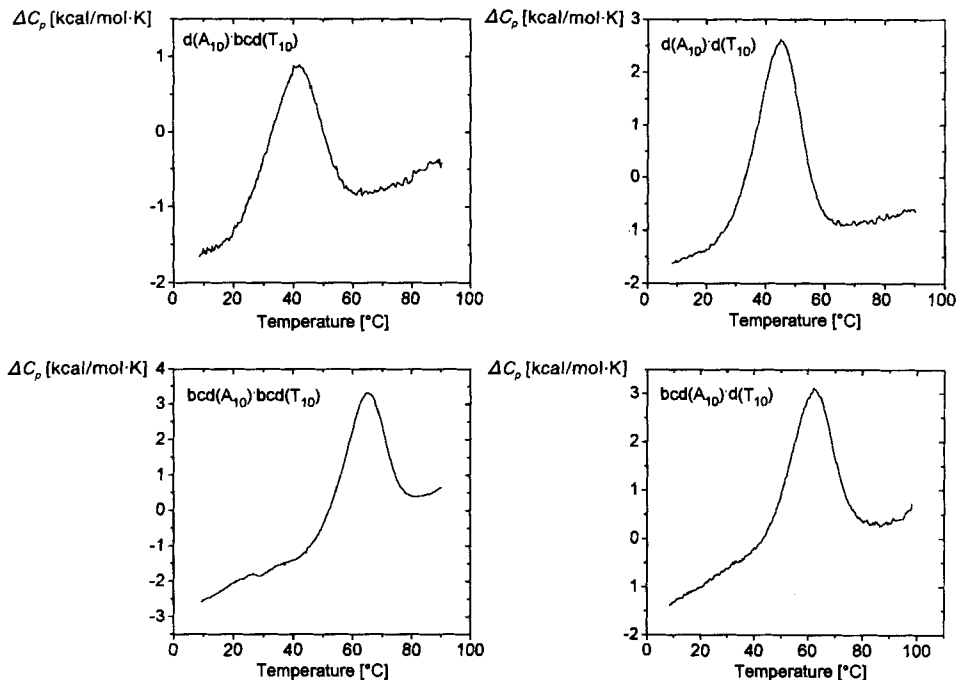


Fig. 11. ΔC_p vs. T plots from DSC: $d(A_{10}) \cdot bcd(T_{10})$ ($c = 0.141$ mM), $d(A_{10}) \cdot d(T_{10})$ ($c = 0.150$ mM), $bcd(A_{10}) \cdot bcd(T_{10})$ ($c = 0.100$ mM), and $bcd(A_{10}) \cdot d(T_{10})$ ($c = 0.133$ mM) in 10 mM NaH_2PO_4 /1M NaCl (pH 7.0)

this duplex melts as a single thermodynamic entity. Surprisingly, in all other cases, ΔH^{DH} is always more negative than ΔH^{DSC} . This is especially pronounced in the case of the bicyclic duplex $bcd(A_{10}) \cdot bcd(T_{10})$ ($\Delta \Delta H = 13.1$ kcal/mol). More negative values of ΔH^{DH} with respect to ΔH^{DSC} , as observed in the cases mentioned, is compatible with the interpretation that the molecularity of the melting process is less than two¹¹⁾. This is in agreement with (concentration-dependent) catenation of the decamers leading to a pseudo-polymeric duplex under the experimental conditions and can also account for the differences between the calorimetric thermodynamic data and those obtained by optical methods [1]. *Breslauer* and coworkers have recently reported a thermodynamic analysis of a 16-mer triplex of 2',5'-linked 3'-deoxyladenylic and 3'-deoxy-2'-oxythymidylic acid [27]. The thermal stability of this triplex was found to be concentration-independent and interpreted as the consequence of a pseudomonomolecular, polymer-like melting process. This triplex showed enhanced thermodynamic stability over its natural analogue although the pairing enthalpy term was less favorable. The similarities in the thermodynamic behavior in this pairing system and bicyclo-DNA suggest a similar structural reason to be operative.

¹¹⁾ From the shape analysis of the DSC curve of $bcd(A_{10}) \cdot bcd(T_{10})$, e.g. ΔH^{DH} can be calculated referring to a bimolecular (-74.6 kcal/mol, see Table 4) or to a (hypothetical) monomolecular process (-51.3 kcal/mol). Since ΔH^{DSC} for this transition is in-between, the molecularity of the process can roughly be interpreted as intermediate between 1 and 2.

4.2.2. *Isothermal Titration Calorimetry*. Isothermal titration calorimetry (ITC) has enormous potential in the determination of thermodynamic data for biomolecular interactions [28]. We found that ITC on a *Omega* titration calorimeter [29] provides a convenient method for the measurement of thermodynamic data of duplex and triplex formation. At constant temperature, a solution containing the receptor molecule in the calorimetric cell is titrated with ligand, and the heat of ligand-to-receptor binding is measured. With this method, it is possible to determine pairing enthalpies and binding constants as well as the stoichiometry of ligand to receptor binding. In a representative experiment, a solution of the purine strand in the calorimetric cell is titrated with aliquots of a solution of the corresponding pyrimidine strand to a final ratio ('A/T') of *ca.* 1:3. After every injection, the heat evolution is measured as a function of time (*Fig. 12*). Normalized ligand-binding enthalpies are then obtained from peak integration over

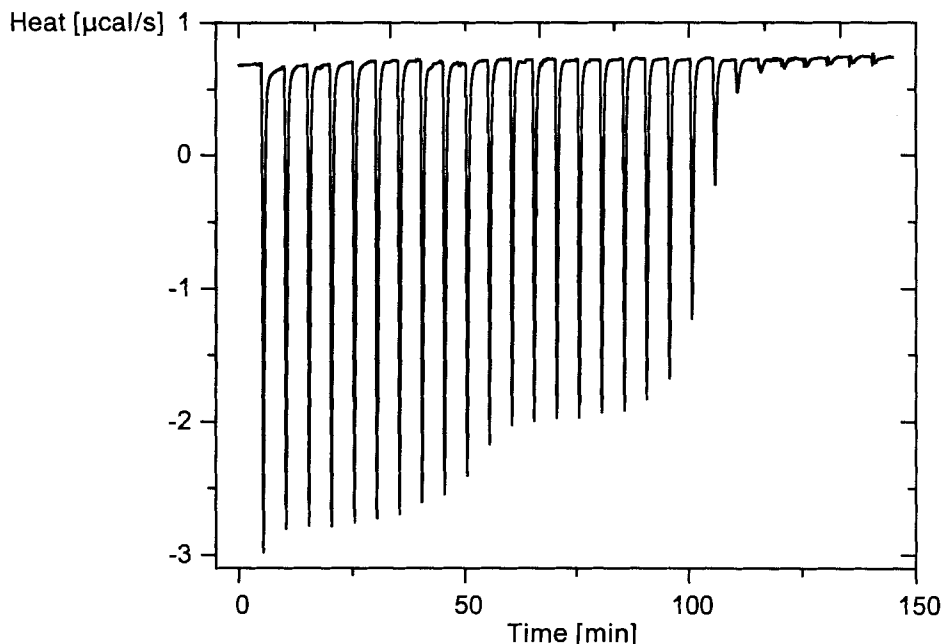


Fig. 12. Isothermal titration calorimetry: heat signal vs. time for the titration of $bcd(A_{10})$ ($c = 16.1 \mu\text{M}$) with $bcd(T_{10})$ ($c = 0.22 \text{ mM}$). At a time interval of 5 min, 28 injections were effected. Buffer: 10 mM $\text{NaH}_2\text{PO}_4/1\text{M NaCl}$, pH 7.0, 9.3°.

the injection signals and are plotted against the molar ratio of ligand to receptor ('T/A' strand, *Fig. 13*).

Binding constants (K) and binding enthalpies (ΔH^{ITC}) of complex formation (*Table 5*) were obtained by curve fitting¹²⁾ taking into consideration two independent consecutive equilibria of the type given in *Eqns. 5* and *6*.

¹²⁾ Curve fitting was performed with the program *MicroCal Origin*TM using the 'two interacting sites' model function. For details, see *Exper. Part*.

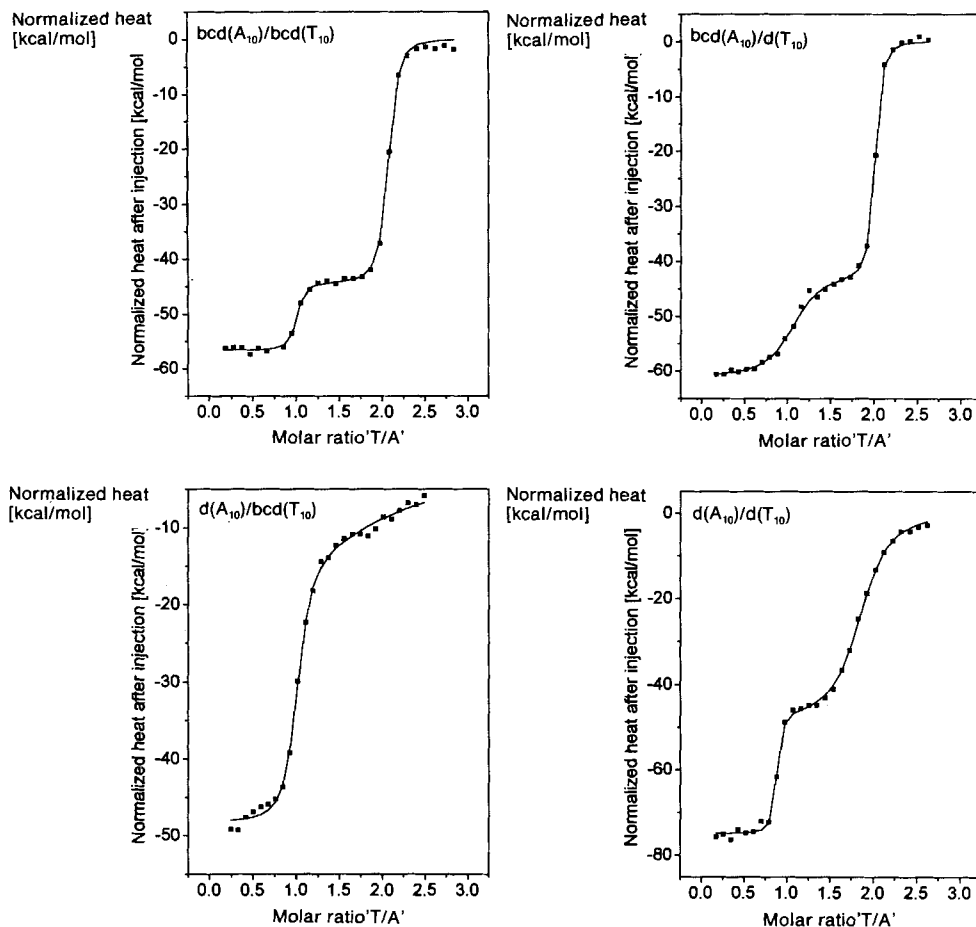


Fig. 13. Isothermal titration calorimetry: normalized heats after injection vs. the molar strand ratio 'T/A'. Exper. conditions: $\text{bcd}(A_{10})/\text{bcd}(T_{10})$: $c(\text{bcd}(A_{10})) = 16.1 \mu\text{M}$, $c(\text{bcd}(T_{10})) = 0.22 \text{ mM}$, $T = 9.3^\circ$; $\text{bcd}(A_{10})/\text{d}(T_{10})$: ($c = \text{bcd}(A_{10}) = 15.7 \mu\text{M}$, $c = (\text{d}(T_{10})) = 0.199 \text{ mM}$, $T = 9.7^\circ$); $\text{d}(A_{10})/\text{bcd}(T_{10})$: $c(\text{d}(A_{10})) = 16.2 \mu\text{M}$, $c(\text{bcd}(T_{10})) = 0.22 \text{ mM}$, $T = 6.6^\circ$; $\text{d}(A_{10})/\text{d}(T_{10})$: $c(\text{d}(A_{10})) = 15.7 \mu\text{M}$, $c(\text{d}(T_{10})) = 0.199 \text{ mM}$, $T = 8.1^\circ$.

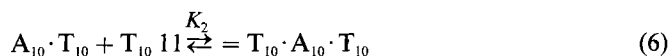
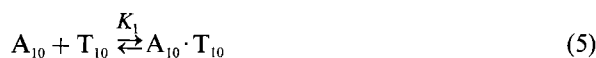
Table 5. Thermodynamic Data for Duplex and Triplex Formation from ITC

		$\text{bcd}(A_{10})/\text{bcd}(T_{10})$ (9.3°) ^a	$\text{d}(A_{10})/\text{d}(T_{10})$ (8.1°) ^a	$\text{bcd}(A_{10})/\text{d}(T_{10})$ (9.7°) ^a	$\text{d}(A_{10})/\text{bcd}(T_{10})$ (6.6°) ^a
Duplex formation	K_1	$1.57 \cdot 10^{10} \pm 8.2 \cdot 10^9$	$2.44 \cdot 10^9 \pm 8.7 \cdot 10^8$	$1.78 \cdot 10^9 \pm 3.8 \cdot 10^8$	$1.56 \cdot 10^7 \pm 1.9 \cdot 10^7$
	$[L \cdot M^{-1}]$				
	ΔH^{ITC}	-56.6 ± 0.3	-74.9 ± 0.3	-61.2 ± 0.4	-48.8 ± 0.4
	$[\text{kcal} \cdot \text{mol}^{-1}]$				
	ΔS^{ITC}	-154 ± 2	-223 ± 3	-174 ± 2	-142 ± 3
	$[\text{cal} \cdot \text{mol}^{-1} \cdot \text{K}^{-1}]$				
	$\Delta G^{\text{ITC}, 25^\circ}$	-10.7 ± 0.9	-8.4 ± 1.2	-9.3 ± 1.0	-6.5 ± 1.3
	$[\text{kcal} \cdot \text{mol}^{-1}]$				

Table 5 (cont.)

		bcd(A ₁₀)/bcd(T ₁₀) (9.3°) ^{a)}	d(A ₁₀)/d(T ₁₀) (8.1°) ^{a)}	bcd(A ₁₀)/d(T ₁₀) (9.7°) ^{a)}	d(A ₁₀)/bcd(T ₁₀) (6.6°) ^{a)}
Triplex formation	<i>K</i> ₂	2.57 · 10 ⁷ ± 3.2 · 10 ⁶	2.43 · 10 ⁶ ± 2.0 · 10 ⁵	5.03 · 10 ⁷ ± 6.3 · 10 ⁶	ca. 5.0 · 10 ⁴
	[l · M ⁻¹]				
	Δ <i>H</i> ^{ITC}	-44.7 ± 0.3	-48.2 ± 0.6	-42.7 ± 0.5	-
	[kcal · mol ⁻¹]				
	Δ <i>S</i> ^{ITC}	-124 ± 2	-142 ± 3.0	-116 ± 2	-
[cal · mol ⁻¹ · K ⁻¹]					
Δ <i>G</i> ^{ITC, 25°}	-7.7 ± 0.9	-5.9 ± 1.4	-8.1 ± 1.1	-	
[kcal · mol ⁻¹]					

^{a)} Titration temp. [°C].



Binding entropies (ΔS^{ITC}) were calculated from the free binding enthalpies (ΔG^{ITC}) that were obtained from the binding constants K at the corresponding temperatures. Tabulated ΔG^{ITC} data (Table 5) were extrapolated to 25°. The ITC curves (Fig. 13) of the three pairing systems d(A₁₀)/d(T₁₀), bcd(A₁₀)/d(T₁₀), and bcd(A₁₀)/bcd(T₁₀) show two distinct binding steps each at molar ratios ('T/A') of 1 and 2, the former indicating duplex and the latter triplex formation. The observation of two isolated binding steps in the system bcd(A₁₀)/d(T₁₀) definitely rules out the possibility of direct triplex formation from the single strands at 1:1 strand stoichiometry, which cannot be excluded completely from the corresponding UV/melting curves (Fig. 7). In the d(A₁₀)/bcd(T₁₀) system, the binding of the second bcd(T₁₀) strand to the d(A₁₀) · bcd(T₁₀) duplex is very weak, as indicated by the broad and incomplete second binding step. The binding constant (Table 5) for the duplex bcd(A₁₀) · bcd(T₁₀) is ca. 10-fold larger than that of natural d(A₁₀) · d(T₁₀) and bcd(A₁₀) · d(T₁₀), and ca. 3 orders of magnitude larger than that of d(A₁₀) · bcd(T₁₀). Third-strand binding is tighter by a factor of 10 in bcd(A₁₀)/d(T₁₀) and bcd(A₁₀)/bcd(T₁₀) and looser by at least 2 orders of magnitude in d(A₁₀)/bcd(T₁₀) relative to the natural systems. Binding enthalpies for third-strand binding (Table 5) are again strongest in the natural system followed by bcd(A₁₀)/bcd(T₁₀) and bcd(T₁₀). The higher thermodynamic stability in the latter two cases, therefore, is also due to a less unfavorable binding entropy term. Interestingly, in bcd(A₁₀)/bcd(T₁₀), the enthalpy and entropy change of third-strand binding amounts of ca. 80% each for that of duplex formation, whereas in the natural system, only ca. 64% each is observed. This indicates that the process of duplex and triplex formation is energetically more degenerate in the bicyclic system.

Entropic stabilization of duplex and triplex formation in the bicyclo-DNA system is best visualized in a ΔG vs. T diagram (Fig. 14) obtained from the enthalpy and entropy data from Table 5 for a temperature interval spanning the physiological relevant range. Since $\Delta G = \Delta H - T\Delta S$, the slopes of the straight lines are directly proportional to ΔS . All duplex pairing systems, where bicyclo-DNA sequences are involved, show ΔG lines with slopes that are less steep than that of the natural reference system. This holds especially

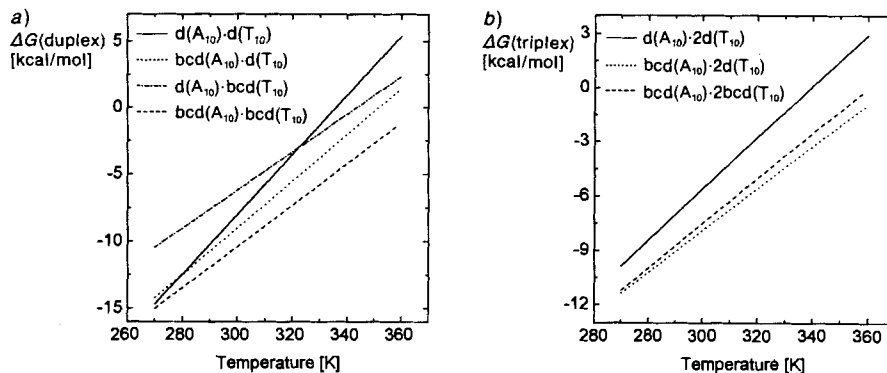


Fig. 14. ΔG vs. T plots for a) duplex formation and b) triplex formation from the thermodynamic data of Table 5

true for the thermodynamically least stable $d(A_{10}) \cdot bcd(T_{10})$ which shows the smallest slope of all duplexes investigated. It is due to the relatively large drop in ΔH that ΔG^{25° of this duplex is less negative than that of the natural duplex. Because of intra-strand base stacking of the adenine bases, an oligonucleotide single strand thereof has an inherently higher structural order than its complementary pyrimidine strand where this interaction is largely lacking. Therefore, one would expect the potential of preorganizing the pyrimidine strand by backbone modification to be higher than in the purine strand. This fits the fact that the entropic contribution to duplex stability (slope in Fig. 14) in $d(A_{10}) \cdot bcd(T_{10})$ is more favorable (less steep) than in $bcd(A_{10})/d(T_{10})$.

Comparison of enthalpies of duplex formation from DSC with those from ITC may establish the contribution of single-strand order to duplex stability. Using data from isothermal batch mixing calorimetry and DSC, it was shown previously in the case of a DNA tridecamer that more than 40% of the total enthalpy stabilizing the duplex state is already present in the constituent single strands [30]. Our studies show that duplex-formation enthalpies from ITC (ΔH^{ITC}) are in all cases *ca.* 5% more negative than those from DSC (ΔH^{DSC}), except for $bcd(A_{10}) \cdot bcd(T_{10})$, where the opposite is observed. Our results, therefore, do not indicate that single-strand order contributes a substantial amount of the enthalpy paid upon duplex melting.

5. Conclusions. – Bicyclo-DNA, having a conformationally more restricted sugar-phosphate backbone, brought about by structural modifications in the sugar part of the nucleoside units, was designed to stabilize duplexation with natural complementary DNA *entropically*¹³⁾. The investigation of the thermodynamic and pairing properties did not only provide experimental proof for the hypothesis underlying the design of this type of nucleosides, but also revealed further important aspects concerning the complex formation of bicyclo-DNA with complementary DNA, namely the marked increase in salt sensitivity of duplex formation with respect to the natural duplex, the pronounced

¹³⁾ In the series of natural oligonucleotide triplexes, thermodynamically more stable complexes due to a more favorable pairing-entropy term are obtained by reducing the molecularity of the complexation as in the case of bimolecular [31] and monomolecular [26b] triplex formation and in complexes involving circular-DNA [32]. Recently, a conformationally restricted riboacetal-DNA analog showing stronger triplex-pairing energy was also reported [33].

preference of a bcdT sequence to bind to complementary RNA although its backbone is restricted to a B (and not A)-like conformation, and the increased triplex stability of bcdA sequences with two T-derived seequences. The fact that an oligonucleotide analogue binds stronger to complementary RNA than DNA is not unprecedented. This was found in the case of *enantio*-DNA [34] and in nucleic-acid analogues containing sulfide bridges [35]. It is clear that the explanation for the origin of the observed pairing behavior of bicyclo-DNA is hidden in the knowledge of its detailed 3-dimensional structure. An indication of possible differences in the backbone structure of duplexes of bicyclo-DNA with itself or with natural DNA as a complement arises from the analysis of the preferred conformation of the nucleosides. Free (deoxy)ribonucleosides show no preference for the torsion angle γ to adopt a value consistent with either the *+sc* or the *ap* orientation¹⁴). In duplexes of the A or B type, γ exclusively has the value for the *+sc* conformation. In the free bicyclodeoxynucleosides [5] and the parallel oriented (C-CH⁺) base-paired miniduplex bcd(C₂) [6], however, the conformation corresponding to γ is preferentially *ap*. To enable duplex formation with γ in the *ap* range, at least one additional change of one of the five remaining torsion angles is necessary. According to the crystal structure of bcd(C₂), this is accomplished by a change of the neighboring torsion angle β from the normal *ap* range (180°) to the *+sc* range (100°). The structural effect of the change in γ is, thereby, mostly compensated by the change in β , resulting in a duplex structure with the helix axis perpendicular to the base plane, and the bases stacked over each other, thus resembling a duplex of the B type [6] [37] (Fig. 15). Whether a similar structural arrangement of the backbone occurs in bicyclo-DNA duplexes with A·T and/or G·C base pairs still needs to be revealed.

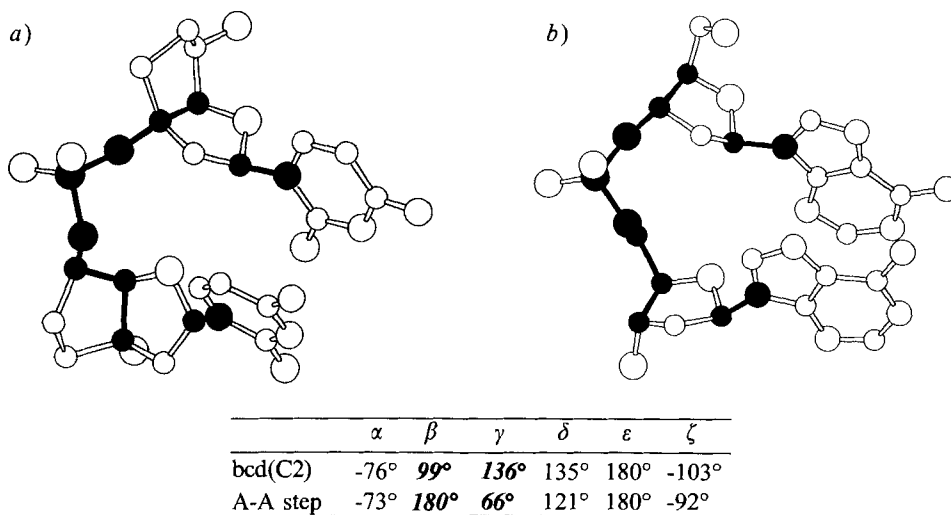


Fig. 15. Comparison of the backbone structures and the torsional angles α - ζ of a) bcd(C₂) [6] and b) the A-A tract of the duplex d(C-G-C-G-A-A-T-T-C-G-C-G) [38] from their X-ray structures

¹⁴) For an overview of the terminology used in the description of nucleic-acid structures, see [36]; *sc* = synclinal, *ap* = antiperiplanar.

The bicyclonucleosides offer some additional structural features that are unique to this class of nucleoside analogues. Inversion of configuration at the center C(5'), e.g., would lead to oligonucleotides that were deprived from the possibility to adopt the natural conformation of torsion angle γ in DNA duplexes of the A or B type. Investigations of the pairing properties of such analogues may help to assess the influence of this torsion angle to the selectivity and the thermodynamic properties of base pairing and may aid in the structure elucidation of the bicyclo-DNA described in this communication. Furthermore, the ethylene bridge between the centers C(3') and C(5') offers a convenient scaffold for introducing functional groups at a unique position. As constituents of an oligomer, such modified nucleosides may have an additional stabilizing effect on duplexation and triplexation and/or may confer (directly or indirectly) chemical reactivity to a target strand bound to it. Experiments in this context are currently under way.

Entropic duplex stabilization is one of the characteristics of homo-DNA [39] and pyranosyl-RNA [40], both containing a conformationally locked pyranose ring in the sugar unit of the corresponding nucleosides. Bicyclo-DNA is an offspring of homo-DNA in that the concept of entropic duplex stabilization by reducing the conformational flexibility in the sugar unit has specifically been implemented in its design.

We gratefully acknowledge financial support from ETH (grant No. 41-2514.5), from the *Swiss National Science Foundation* (grant No. 21-36603.92), and from the *Stipendienfonds der Basler Chemischen Industrie*. We thank Prof. A. Eschenmoser for continuing encouragement, Prof. P. Luisi for the opportunity to record CD spectra, the late Dr. J. Schreiber for help with HPLC and *Ciba-Geigy AG*, Basel, for equipping us with the DSC and ITC calorimeters.

Experimental Part

General. For reagents, solvents, and analytical instrumentation used in the synthesis and characterization of monomer building blocks, see [5]. Phosphodiesterase from *Crotalus durissus* (EC 3.1.15.1) and alkaline phosphatase from calf intestine (EC 3.1.3.1) were from *Böhringer*, Mannheim. HPLC: *Pharmacia-LKB-2249* gradient system attached to an *ABI-Kratos-Spectroflow-757* UV/VIS detector and a *Tarkan W + W* recorder 600 or *HP-3396A* integrator. Extinction coefficients: ϵ of oligonucleotides according to [41] by relating the UV absorption of an aliquot of the oligonucleotide soln. (10 mM *Tris* · HCl, 25°) at 260 nm with that of the free monomeric units after complete digestion of the aliquot with snake-venom phosphodiesterase/alkaline phosphatase (HPLC control), i.e. $\epsilon = (10 \cdot D \cdot \epsilon_{\text{mono}}) / D_{\text{mono}}$, with D and D_{mono} = absorption of oligomer and free nucleoside, resp., and ϵ and ϵ_{mono} = corresponding extinction coefficients; $\epsilon = 107000$ (d(A₁₀)), 105000 (bcd(A₁₀)), 96000 (d(T₁₀)), and 88000 (bcd(T₁₀)). CD Spectra: *Jasco J-600* spectropolarimeter connected to an *IBM AT* personal computer; thermostating of the cell holder by a *Haake* circulating bath, temp. determination directly in the sample soln.

UV/Melting Curves. *Varian-Cary-3E* UV/VIS spectrometer equipped with a temp.-controller unit and connected to a *Compaq-ProLinea-3/25-zs* personal computer; temp. gradients of 0.5°/min, data points collected in intervals of ca. 0.3°; at temp. < 20°, the cell compartment was flushed with N₂ to avoid condensation of H₂O on the UV cells; % hyperchrom.(wavelength) = 100 · [D(T) - D₀] / D₀ with D(T) = absorption at temp. T and D₀ = lowest absorption in the temp. interval; the transition temperature T_m was determined as described [25b].

Differential Scanning Calorimetry (DSC). *MicroCal-2* differential-scanning calorimeter (*MicroCal Inc.*, Northampton, MA, U.S.A.) connected to a *Grant-LTD-6* cooling device, interfaced to a *Gateway-2000-386/33* personal computer and controlled by the *Origin v. 2.90* software; sample cell vol. 1.2186 ml, scan rate 90°/h. Desalted and lyophilized duplex samples were dissolved in degassed buffer (10 mM NaH₂PO₄/1M NaCl, pH 7.0) to a conc. of 0.13–0.15 mM and transferred to the sample cell and measured against buffer as the reference. Data acquisition was performed with the *Origin* software. Baselines (buffer/buffer) were recorded either directly before or after an experiment and subtracted. Reversibility was checked by running at least 4 scans. All experiments were performed in duplicate.

Isothermal Titration Calorimetry (ITC). Omega isothermal titration calorimeter (MicroCal Inc., Northampton, MA, U.S.A.); cooling device, interface, and control as described for DSC. All measurements were performed in 10 mM $\text{NaH}_2\text{PO}_4/1\text{M NaCl}$, pH 7.0. Sample-cell vol. 1.3267 ml. The soln. of the purine strand (15–20 μM) was placed in the cell and the titrant soln. (pyrimidine strand, 0.19–0.23 mM) in a 250- μl precision syringe, whose needle was paddle-shaped and rotated at 400 rpm. The syringe plunger was mechanically coupled to a stepping motor that was computer-controlled. Aliquots of 8–15 μl were added. Typically 15–28 injections amounting to a total of 2.5–3 equiv. of titrand were added. A 5-min time interval between two injections was allowed for the systems to equilibrate. The integrated heats produced by such pulses were fitted by the Origin software using the multiple interacting site fitting function. All ITC experiments were performed in duplicate.

(4,4'-Dimethoxytriphenyl)methyl Trifluoromethanesulfonate. A soln. of (4,4'-dimethoxytriphenyl)methyl chloride (5.8 g, 17.1 mmol) in THF (25 ml) was added under Ar at r.t. to a stirred soln. of $\text{Ag}(\text{CF}_3\text{SO}_3)$ (4.4 g, 17.1 mmol) in THF (20 ml). After 1 h, the white precipitate formed (AgCl) was filtered off under Ar and washed with THF (50 ml) and the filtrate concentrated to ca. 15 ml. The dark purple mash was dissolved in CH_2Cl_2 (30 ml) and Et_2O (30 ml) and kept at -20° for 16 h. After addition of a 2nd portion of Et_2O (100 ml) and waiting for another 30 min, the dark needles were collected under Ar, washed with Et_2O (50 ml), and dried (r.t./high vacuum, 3 h): 6.35 g (82%) of $[(\text{MeO})_2\text{Tr}]\text{CF}_3\text{SO}_3$. $^{13}\text{C-NMR}$ (75 MHz, CDCl_3): 57.6 (*q*, MeO); 123.0 (*q*, CF_3); 117.5, 129.5, 137.6, 138.0, 144.5 (*5d*, arom. C); 132.4, 139.0, 172.5, 194.6 (*4s*, arom. C). Anal. calc. for $\text{C}_{22}\text{H}_{19}\text{F}_3\text{O}_3\text{S}$: C 58.40, H 4.23, F 12.60, O 17.68, S 7.09; found: C 57.98, H 4.21, F 12.44, S 7.05.

Tritylation: General Procedure. To a soln. of bicyclocloxy nucleoside derivative **1** or **5–7** in pyridine or 2,6-dimethylpyridine/ CH_2Cl_2 1:1 (0.06–0.3M) was added $[(\text{MeO})_2\text{Tr}]\text{CF}_3\text{SO}_3$ (1.5–2.6 equiv.) under Ar at r.t. If necessary, further reagent (0.6–3.3 equiv.) was gradually added until all starting material had disappeared (TLC control). After 3–6.5 h, the reaction was quenched by addition of sat. NaHCO_3 soln. and the resulting mixture extracted with CH_2Cl_2 or AcOEt. The org. phase was dried (MgSO_4) and evaporated and the corresponding crude tritylated product **8–11** purified by CC.

(3'S,5'R)-1-{2'-Deoxy-5'-O-[(4,4'-dimethoxytriphenyl)methyl]-3',5'-ethano- β -D-ribofuranosyl}thymine (8). From **1** (305 mg, 1.137 mmol), pyridine (0.19M), and $[(\text{MeO})_2\text{Tr}]\text{CF}_3\text{SO}_3$ (772 mg, 1.706 mmol + 0.5 equiv. after 105 min + 0.12 equiv. after 165 min; total reaction time 5.25 h). CC (silica gel, hexane/AcOEt 1:9) followed by crystallization from AcOEt/hexane gave **8** (570 mg, 88%). Fine colorless needles. TLC (hexane/AcOEt 1:9): R_f 0.37. $^1\text{H-NMR}$ (300 MHz, CDCl_3): 1.22–1.36, 1.70–1.82 (*2m*, 1 H–C(2'), 2 H–C(6'), 2 H–C(7')); 1.76 (*d*, $J = 1.1$, Me–C(5)); 2.62 (*dd*, $J = 5.1$, 13.8, 1 H–C(2'')); 3.31 (*br. s*, OH); 3.75 (*d*, $J = 6.4$, H–C(4')); 3.78 (*s*, 2 MeO); 3.94 (*dd*, $J = 7.0$, 13.6, H–C(5'')); 6.35 (*dd*, $J = 5.2$, 9.3, H–C(1'')); 6.82 (*dd*, $J = 1.3$, 9.0, 4 arom. H); 7.18–7.31, 7.38–7.43 (*2m*, 7 arom. H); 7.52 (*d*, $J = 7.0$, 2 arom. H); 7.80 (*d*, $J = 1.1$, H–C(6)); 9.27 (*br. s*, NH). $^{13}\text{C-NMR}$ (75 MHz, CDCl_3): 12.46 (*q*, Me–C(5)); 31.30, 34.48 (*2t*, C(6'), C(7')); 47.44 (*t*, C(2'')); 55.25 (*q*, MeO); 73.35 (*d*, C(5'')); 85.46, 88.89 (*2d*, C(1'), C(4'')); 86.20, 87.22 (*2s*, C(3'), Ar_2CPh); 111.32 (*s*, C(5)); 113.21, 126.95, 127.90, 128.16, 130.16 (*5d*, arom. C); 135.44 (*d*, C(6)); 136.61, 136.77, 145.54 (*3s*, arom. C); 150.46 (*s*, C(2)); 158.68 (*s*, arom. C); 163.76 (*s*, C(4)). FAB-MS (*pos.*): 593 (7.4, $[M + 23]^+$), 304 (37), 303 (100), 135 (11), 77 (10).

(3'S,5'R)-N⁶-Benzoyl-9-{2'-deoxy-5'-O-[(4,4'-dimethoxytriphenyl)methyl]-3',5'-ethano- β -D-ribofuranosyl}adenine (9). From **5** (505 mg, 1.32 mmol), pyridine (0.13M), and $[(\text{MeO})_2\text{Tr}]\text{CF}_3\text{SO}_3$ (1.198 g, 2.64 mmol + 3.3 equiv. after 30 min; total reaction time 3 h). CC (silica gel, AcOEt, then $\text{CH}_2\text{Cl}_2/\text{MeOH}$ 9:1) gave **9** (770 mg, 85%). Slightly yellowish foam. TLC (AcOEt): R_f 0.37. $^1\text{H-NMR}$ (400 MHz, CDCl_3): 1.28–1.36, 1.50–1.60, 1.83–1.88 (*3m*, 2 H–C(6'), 2 H–C(7'')); 2.35 (*dd*, $J = 8.7$, 13.7, 1 H–C(2'')); 2.70 (*br. s*, OH); 2.81 (*dd*, $J = 5.5$, 13.7, 1 H–C(2'')); 3.72 (*d*, $J = 5.9$, H–C(4'')); 3.77 (*s*, 2 MeO); 3.89–3.95 (*m*, H–C(5'')); 6.43 (*dd*, $J = 5.5$, 8.7, H–C(1'')); 6.81 (*d*, $J = 8.6$, 4 arom. H); 7.17–7.21 (*m*, 1 arom. H); 7.24–7.28 (*m*, 2 arom. H); 7.38–7.42 (*m*, 4 arom. H); 7.50–7.54 (*m*, 4 arom. H); 7.57–7.69 (*m*, 1 arom. H); 8.04 (*d*, $J = 7.2$, 2 arom. H); 8.51, 8.79 (*2s*, H–C(2), H–C(8)); 9.17 (*br. s*, NH). $^{13}\text{C-NMR}$ (100 MHz, CDCl_3): 30.79, 35.23 (*2t*, C(6'), C(7'')); 48.90 (*t*, C(2'')); 55.24 (*q*, MeO); 73.50 (*d*, C(5'')); 85.13, 89.05 (*2d*, C(1'), C(4'')); 86.23, 87.10 (*2s*, C(3'), Ar_2CPh); 123.20 (*s*, C(5)); 113.18, 126.89, 127.91, 128.19, 128.88, 130.16, 132.79 (*7d*, arom. C); 133.75, 136.73, 136.81 (3s, arom. C); 141.18 (*d*, C(8)); 145.52 (*s*, arom. C); 149.44, 151.34 (*2s*, C(4), C(6)); 152.62 (*d*, C(2)); 158.62 (*s*, arom. C); 164.67 (*s*, CO). FAB-MS (*pos.*): 806 (18, $[M + 23]^+$), 684 (5, $[M + 11]^+$), 683 (0.9, M^+), 304 (37), 303 (100), 242 (24), 240 (31), 105 (26), 77 (10).

(3'S,5'R)-N⁴-Benzoyl-1-{2'-deoxy-5'-O-[(4,4'-dimethoxytriphenyl)methyl]-3',5'-ethano- β -D-ribofuranosyl}cytosine (10). From **6** (1.17 g, 3.27 mmol), 2,6-dimethylpyridine/ CH_2Cl_2 1:1 (0.07M), and $[(\text{MeO})_2\text{Tr}]\text{CF}_3\text{SO}_3$ (2.22 g, 4.91 mmol, 1.5 equiv.); 4 H). CC (silica gel, AcOEt) gave **10** (1.96 g, 91%). Colorless foam. TLC ($\text{CH}_2\text{Cl}_2/\text{MeOH}$ 10:1): R_f 0.60. $^1\text{H-NMR}$ (400 MHz, CDCl_3): 1.29–1.37, 1.43–1.49 (*2m*, 2 H–C(6'), 2 H–C(7'')); 1.75 (*dd*, $J = 8.3$, 14.0, 1 H–C(2'')); 3.04 (*dd*, $J = 5.5$, 14.2, 1 H–C(2'')); 3.69 (*d*, $J = 6.4$, H–C(4'')); 3.81 (*s*, 2 MeO); 3.91–3.98 (*m*, H–C(5'')); 6.33 (*dd*, $J = 5.6$, 8.1, H–C(1'')); 6.83–6.88, 7.21–7.25, 7.30–7.33, 7.40–7.45, 7.49–7.54,

7.59–7.63, 7.90–7.92 (7*m*, 19 H, arom. H, H–C(5)); 8.76 (*d*, *J* = 7.5, H–C(6)). ¹³C-NMR (100 MHz, CDCl₃): 31.2, 34.2 (2*t*, C(6'), C(7')); 49.0 (*t*, C(2')); 55.3 (*q*, MeO); 73.4 (*d*, C(5')); 86.5, 87.5 (2*s*, C(3'), Ar₃C); 87.9, 89.3 (2*d*, C(1'), C(4')); 96.8 (*d*, C(5)); 113.2, 127.0, 127.6, 127.9, 128.2, 129.0, 130.22, 130.224 (8*d*, arom. C); 133.2, 136.6, 136.7, 145.5, 158.7 (5*s*, arom. C); 145.1 (*d*, C(6)); 162.3 (*s*, C(4)). FAB-MS (pos.): 660 (0.005, [*M* + 1]⁺), 659 (0.003, *M*⁺), 305 (11), 304 (58), 303 (86), 288 (12), 273 (12), 227 (18), 215 (24), 214 (14).

(3'*S*,5'*R*)-9-{2'-Deoxy-5'-O-[(4,4'-dimethoxytriphenyl)methyl]-3',5'-ethano-β-D-ribofuranosyl}-N²-isobutyl-tyranyl-guanine (**11**). From **7** (221 mg, 0.608 mmol), pyridine (0.30*M*), and [(MeO)₂Tr]CF₃SO₃ (413 mg, 0.912 mmol, 1.5 equiv. + 0.5 equiv. after 2 h + 0.5 equiv. after 4 h; total reaction time 6.5 h). CC (silica gel, CH₂Cl₂/MeOH 20:1, 2% Et₃N) and precipitation from Et₂O at r.t. gave **11** (313 mg, 77%). White powder. TLC (CH₂Cl₂/MeOH 10:1): *R*_f 0.57. ¹H-NMR (400 MHz, CDCl₃): 1.10–1.25, 1.68–1.70 (2*m*, Me₂CH, 2 H–C(6'), 2 H–C(7')); 2.04–2.10, 2.55–2.58 (2*m*, 2 H–C(2')); 2.81–2.88 (*m*, Me₂CH); 3.69, 3.70 (2*s*, 2 MeO); 3.88–3.90 (*m*, H–C(4'), H–C(5')); 4.40 (br. *s*, OH); 6.02–6.06 (*m*, H–C(1')); 6.73 (*dd*, *J* = 7.6, 8.9, 4 arom. H); 7.11 (*t*, *J* = 7.3, 1 arom. H); 7.16–7.20 (*m*, 2 arom. H); 7.33–7.36 (*m*, 4 arom. H); 7.46 (*d*, *J* = 7.3, 2 arom. H); 8.16 (*s*, H–C(8)); 10.9, 12.3 (br. 2*s*, 2 NH). ¹³C-NMR (100 MHz, CDCl₃): 19.02, 19.04 (2*q*, Me₂CH); 30.8, 34.6 (2*t*, C(6'), C(7')); 36.0 (*d*, Me₂CH); 48.5 (*t*, C(2')); 55.16, 55.17 (2*s*, MeO); 73.5 (*d*, C(5')); 85.4, 89.5 (2*d*, C(1'), C(4')); 85.8, 87.0 (2*s*, Ar₂CPh, C(3')); 113.10, 113.13, 126.8, 127.8, 128.2, 130.1, 130.2 (7*d*, arom. C); 120.5 (*s*, C(5)); 136.7, 137.0, 145.6, 148.3, 148.5 (5*s*, arom. C, C(2), C(4')); 137.1 (*d*, C(8)); 156.2 (*s*, C(6)); 158.5, 158.6 (2*s*, arom. C); 180.3 (*s*, CO). FAB-MS (pos.): 666 (5, [*M* + 1]⁺), 665 (1, *M*⁺), 304 (30), 303 (100), 222 (12).

Phosphoramidites: General Procedure. To a soln. (or suspension) of each tritylated bicyclic deoxynucleoside derivative **8–11** in THF or MeCN (0.1–0.175*M*) were added at r.t. under Ar ((i-Pr)₂EtN (4–6 equiv.) and chloro(2-cyanoethoxy)(diisopropylamino)phosphine (2–3 equiv.). After completion of the reaction (1–3 h, TLC control), sat. NaHCO₃ soln. was added and the resulting mixture extracted with AcOEt. The org. phase was dried (MgSO₄) and evaporated and the corresponding crude phosphoramidite **12–15** purified by CC followed by precipitation.

(3'*S*,5'*R*)-1-{3'-O-[(2-Cyanoethoxy)(diisopropylamino)phosphino]-2'-deoxy-5'-O-[(4,4'-dimethoxytriphenyl)methyl]-3',5'-ethano-β-D-ribofuranosyl}thymine (**12**). From **8** (200 mg, 0.35 mmol), THF (2 ml), ((i-Pr)₂EtN (360 μl, 2.103 mmol), and chloro(2-cyanoethoxy)(diisopropylamino)phosphine (235 μl, 1.053 mmol). CC (silica gel, hexane/AcOEt 1:2, 3% Et₃N) and precipitation from pentane at 0° gave **12** (171 mg, 63%). White powder (1:1 mixture by ¹H-NMR). TLC (hexane/AcOEt 1:4): *R*_f 0.64. ¹H-NMR (400 MHz, CDCl₃): 1.12–1.18 (*m*, Me₂CH); 1.22–1.32, 1.51–1.65 (2*m*, 2 H–C(6'), 2 H–C(7')); 1.70, 1.76 (2*d*, *J* = 1.1, Me–C(5)); 1.84–1.94 (*m*, 1 H–C(2')); 2.58–2.67 (*m*, OCH₂CH₂N); 2.91–2.99 (*m*, 1 H–C(2')); 3.56–3.70, 3.72–3.82 (2*m*, Me₂CH, OCH₂CH₂N); 3.80, 3.81 (2*s*, 2 MeO); 3.90–3.98 (*m*, H–C(4'), H–C(5')); 6.28 (*m*, H–C(1')); 6.83–6.86 (*m*, 4 arom. H); 7.21–7.39 (*m*, 3 arom. H); 7.40–7.44 (*m*, 4 arom. H); 7.52, 7.54 (2*d*, *J* = 1.3, 2 arom. H); 7.80, 7.82 (2*d*, *J* = 1.2, H–C(6)); 8.54 (br. *s*, NH). ¹³C-NMR (100 MHz, CDCl₃): 12.39, 12.49 (2*q*, Me–C(5)); 20.21, 20.28, 20.36 (3*t*, OCH₂CH₂N); 24.22, 24.30, 24.51, 24.55, 24.57, 24.61 (6*q*, Me₂CH); 31.14, 31.37 (2*t*, C(6')); 33.0, 33.49 (2*td*, *J*(C,P) = 10, C(7')); 43.32 (*dd*, *J*(C,P) = 2, Me₂CH); 43.44 (*d*, Me₂CH); 45.77, 45.90 (2*td*, *J*(C,P) = 7, C(2')); 55.26 (*q*, MeO); 57.78, 57.96 (2*td*, *J*(C,P) = 9, OCH₂CH₂N); 72.79, 72.90 (2*d*, C(5')); 85.64, 85.69 (2*d*, C(1')); 87.32, 87.36 (2*s*, Ar₂CPh); 88.07, 88.40 (2*dd*, *J*(C,P) = 7, H–C(4')); 90.31, 90.41 (2*sd*, *J*(C,P) = 10, C(3')); 111.02, 111.06 (2*s*, C(5)); 113.22, 113.23 (2*d*, arom. C); 117.68, 117.85 (2*s*, CN); 126.97, 127.00, 127.95, 128.13, 128.19, 130.20 (6*d*, arom. C); 135.51, 135.63 (2*d*, C(6)); 136.49, 136.54, 136.67, 136.70, 145.45, 145.50 (6*s*, arom. C); 150.07, 150.14 (2*s*, C(2)); 158.70 (*s*, arom. C); 163.70 (*s*, C(4)). ³¹P-NMR (161.9 MHz, CDCl₃): 141.97, 142.59.

(3'*S*,5'*R*)-N⁶-Benzoyl-9-{3'-O-[(2-cyanoethoxy)(diisopropylamino)phosphino]-2'-deoxy-5'-O-[(4,4'-dimethoxytriphenyl)methyl]-3',5'-ethano-β-D-ribofuranosyl}adenine (**13**). From **9** (998 mg, 1.46 mmol), MeCN (15 ml), ((i-Pr)₂EtN (1 ml, 5.841 mmol), and chloro(2-cyanoethoxy)(diisopropylamino)phosphine (650 μl, 2.914 mmol). CC (silica gel, hexane/AcOEt 1:4) gave **13** (980 mg, 76%). White foam (1:1 mixture by ¹H-NMR). TLC (hexane/AcOEt 1:4): *R*_f 0.55. ¹H-NMR (400 MHz, CDCl₃): 1.13–1.18 (*m*, Me₂CH); 1.30–1.39, 1.52–1.72, 1.84–1.95 (3*m*, 2 H–C(6'), 2 H–C(7')); 2.26–2.35 (*m*, OCH₂CH₂N); 2.57–2.67 (*m*, 1 H–C(2'), OCH₂CH₂N); 3.12–3.19 (*m*, 1 H–C(2')); 3.55–3.74 (*m*, Me₂CH, OCH₂CH₂N); 3.75–3.82 (*m*, Me₂CH); 3.78, 3.79 (2*s*, 2 MeO); 3.86–3.96 (*m*, H–C(4'), H–C(5')); 6.42 (*m*, H–C(1')); 6.80–6.84, 7.19–7.22, 7.25–7.30, 7.38–7.44, 7.50–7.55, 7.60–7.63 (6*m*, arom. H); 8.04 (*d*, *J* = 7.2, arom. H); 8.50, 8.51, 8.81, 8.82 (4*s*, H–C(2), H–C(8)); 9.07 (br. *s*, NH). ¹³C-NMR (100 MHz, CDCl₃): 20.29, 20.37 (2*t*, OCH₂CH₂N); 24.27, 24.35, 24.53, 24.56, 24.59, 24.62 (6*q*, Me₂CH); 30.41, 30.63 (2*t*, C(6')); 33.43, 33.83 (2*td*, *J*(C,P) = 10, C(7')); 43.37, 43.50 (2*dd*, *J*(C,P) = 3.5, Me₂CH); 47.41, 47.63 (2*td*, *J*(C,P) = 7, C(2')); 55.24 (*q*, MeO); 57.78, 57.96 (2*td*, *J*(C,P) = 12, OCH₂CH₂N); 73.09, 73.19 (2*d*, C(5')); 85.20 (*d*, C(1')); 87.10, 87.13 (2*s*, Ar₂CPh); 88.12, 88.48 (2*dt*, *J*(C,P) = 7, C(4')); 90.10, 90.19 (2*sd*, *J*(C,P) = 9, C(3')); 113.18 (*d*, arom. C); 117.56, 117.62 (2*s*, CN); 123.25, 123.29 (2*s*, C(5)); 126.78, 127.86, 127.89, 128.20, 128.22, 128.89, 130.20, 132.74 (8*d*, arom. C); 133.81, 133.84, 136.75, 136.77, 136.83 (5*s*, arom. C); 141.21,

141.31 (2*d*, C(8)); 145.56 (*s*, arom. C); 149.37 (*s*, C(4)); 151.49 (*s*, C(6)); 152.67 (*d*, C(2)); 158.62 (*s*, arom. C); 164.58 (*s*, CO). ³¹P-NMR (161.9 MHz, CDCl₃): 142.31, 142.74. FAB-MS (pos.): 884 (1.0, [M + 1]⁺), 304 (38), 303 (100), 240 (22), 201 (14), 105 (17).

(3'*S*,5'*R*)-N⁴-Benzoyl-1-{3'-O-[(2-cyanoethoxy)(diisopropylamino)phosphino]-2'-deoxy-5'-O-[(4,4'-dimethoxytriphenyl)methyl]-3',5'-ethano-β-D-ribofuranosyl}cytosine (**14**). From **10** (500 mg, 0.76 mmol), THF (5 ml), (i-Pr)₂EtN (520 μl, 3.03 mmol), and chloro(2-cyanoethoxy)(diisopropylamino)phosphine (340 μl, 1.52 mmol). CC (silica gel, hexane/AcOEt 1:2, 1.5% Et₃N) and precipitation from hexane at 0° gave **14** (473 mg, 75%). Fine white powder (1:1 mixture by ¹H-NMR). TLC (hexane/AcOEt 1:2): R_f 0.48. ¹H-NMR (400 MHz, CDCl₃): 1.104, 1.139, 1.143, 1.148 (4*d*, *J* = 6.8, Me₂CH); 1.39–1.66, 1.68–1.75 (2*m*, 2 H–C(6'), 2 H–C(7')); 1.80–1.89 (*m*, 1 H–C(2'')); 2.59 (*dd*, *J* = 6.6, 12.8, 1 H, OCH₂CH₂CN); 2.64 (*t*, *J* = 6.4, 1 H, OCH₂CH₂CN); 3.22–3.29 (*m*, 1 H–C(2'')); 3.52–3.61 (*m*, Me₂CH); 3.61–3.80 (*m*, H–C(4'), OCH₂CH₂CN); 3.82 (*s*, MeO); 3.90–3.95 (*m*, H–C(5'')); 6.15–6.21 (*m*, H–C(1'')); 6.85–6.88, 7.23–7.27, 7.31–7.35, 7.40–7.46, 7.50–7.55, 7.59–7.63 (6*m*, 17 H, arom. H, H–C(5)); 7.91 (*d*, *J* = 7.5, 2 arom. H); 8.64 (*br. s*, NH); 8.75 (*d*, *J* = 7.4, H–C(6)). ¹³C-NMR (100 MHz, CDCl₃): 20.1, 20.2, 20.3 (3*t*, OCH₂CH₂CN); 24.2, 24.3, 24.50, 24.56, 24.61 (5*q*, Me₂CH); 30.8, 31.1 (2*t*, C(6')); 32.75, 33.35 (2*td*, *J*(C,P) = 10, C(7'')); 43.40 (*dd*, *J*(C,P) = 12.6, Me₂CH); 43.43 (*dd*, *J*(C,P) = 12.8, Me₂CH); 47.55 (*td*, *J*(C,P) = 10, C(2'')); 47.9 (*t*, C(2'')); 55.3 (*q*, MeO); 57.8 (*dt*, *J*(C,P) = 5.9, OCH₂CH₂CN); 58.0 (*dt*, *J*(C,P) = 6.2, OCH₂CH₂CN); 72.9, 73.2 (2*d*, C(5'')); 87.6, 87.7 (2*s*, Ar₂CPh); 88.0, 88.1, 88.4, 88.5 (4*d*, C(1'), C(4'')); 90.65, 90.75 (2*sd*, *J*(C,P) = 10, C(3'')); 96.5 (*s*, C(5)); 113.2, 127.1, 127.6, 128.0, 128.1, 128.2, 129.1, 130.3, 133.1 (9*d*, arom. C); 117.6, 117.8 (2*s*, CN); 136.49, 136.52, 136.6, 145.4, 145.5, 158.8 (6*s*, arom. C); 145.1 (*s*, C(6)); 162.1 (*s*, C(4)). ³¹P-NMR (161.9 MHz, CDCl₃): 142.8, 142.0. FAB-MS (pos.): 882 (0.5, [M + 22]⁺), 860 (0.5, [M + 1]⁺), 752 (0.5), 642 (2), 485 (2), 453 (1), 337 (8), 304 (37), 303 (100), 216 (11), 105 (16).

(3'*S*,5'*R*)-9-{3'-O-[(2-Cyanoethoxy)(diisopropylamino)phosphino]-2'-deoxy-5'-O-[(4,4'-dimethoxytriphenyl)methyl]-3',5'-ethano-β-D-ribofuranosyl}-N²-isobutrylguanidine (**15**). From **11** (719 mg, 1.08 mmol), THF (10 ml), (i-Pr)₂EtN (750 μl, 4.32 mmol), and chloro(2-cyanoethoxy)(diisopropylamino)phosphine (490 μl, 2.16 mmol). CC (AcOEt) gave **15** (880 mg, 94%). White foam (*ca.* 1:1 mixture by ¹H-NMR). The anal. data are from material of an analogous experiment, where **15** was precipitated from pentane at 0° (43%), after CC. TLC (hexane/AcOEt 1:2): R_f 0.25. ¹H-NMR (400 MHz, CDCl₃): 1.09–1.15, 1.21–1.24 (2*m*, Me₂CH); 1.42–1.58, 1.82–1.95 (2*m*, 2 H–C(6'), 2 H–C(7'')); 2.04 (*dd*, *J* = 8.8, 13.8, 0.4 H, H–C(2'')); 2.12 (*dd*, *J* = 9.1, 14.1, 0.6 H, H–C(2'')); 2.52–2.59 (*m*, 1 H, Me₂CH); 2.62–2.71 (*m*, 2 H, OCH₂CH₂CN); 3.08 (*dd*, *J* = 5.3, 15.2, 0.6 H, H–C(2'')); 3.17–3.21 (*m*, 0.4 H, H–C(2'')); 3.48 (*d*, *J* = 6.1, 0.4 H, H–C(4'')); 3.50–3.61 (*m*, 2 H, Me₂CH); 3.62–3.69 (*m*, H–C(5'')); 3.791, 3.795 (2*s*, 2 MeO); 3.81–3.89 (*m*, OCH₂CH₂CN); 3.92 (*dd*, *J* = 2.9, 6.0, 0.6 H, H–C(4'')); 6.05 (*dd*, *J* = 5.2, 8.7, 0.4 H, H–C(1'')); 6.17 (*dd*, *J* = 5.4, 9.0, 0.6 H, H–C(1'')); 6.80–7.00, 7.18–7.23, 7.27–7.31, 7.39–7.44, 7.51–7.55 (5*m*, arom. H); 8.14 (*s*, 0.6 H, H–C(8)); 8.18 (*s*, 0.4 H, H–C(8)); 8.97, 9.20, 11.95 (3 *br. s*, NH). ¹³C-NMR (100 MHz, CDCl₃): 18.81, 18.87, 18.94, 19.0 (4*q*, Me₂CH); 20.4, 20.5 (2*td*, *J*(C,P) = 7.7, OCH₂CH₂CN); 24.24, 24.28, 24.33, 24.36, 24.48, 24.51, 24.54 (7*q*, Me₂CH); 29.8, 31.0 (2*t*, C(6')); 33.43, 34.59 (2*td*, *J*(C,P) = 6, C(7'')); 36.1, 36.3 (2*d*, Me₂CH); 43.28, 43.40 (2*dd*, *J*(C,P) = 6, Me₂CH); 47.6 (*td*, *J*(C,P) = 6.8, C(2'')); 48.0 (*td*, *J*(C,P) = 5.9, C(2'')); 55.2 (*q*, MeO); 72.8, 73.5 (2*d*, C(5'')); 85.1, 85.2, 85.5, 86.7, 86.8, 88.97, 89.01 (7*d*, C(1'), C(4'')); 87.0 (*s*, Ar₂CPh); 90.37 (*d*, *J*(C,P) = 11.1, C(3'')); 90.41 (*d*, *J*(C,P) = 8.6, C(3'')); 113.2, 126.87, 126.91, 127.9, 128.2, 128.3, 130.20, 130.24 (8*d*, arom. C); 117.9, 118.1 (2*s*, CN); 121.5 (*s*, C(5)); 136.5, 136.6 (2*d*, C(8)); 136.8, 147.5, 147.57, 147.62, 158.6, 158.7 (7*s*, arom. C(2), C(4)); 155.66, 155.71 (2*s*, C(6)); 178.6, 178.8 (2*s*, CO). ³¹P-NMR (161.9 MHz, CDCl₃): 141.9, 142.3. FAB-MS (pos.): 866 (2, [M + 1]⁺), 304 (35), 303 (100), 222 (10).

Active Esters 16–19: General Procedure. To a soln. of each nucleoside derivative **8–11** in pyridine (0.18–0.2M) were added succinic anhydride (10 equiv.) and, after cooling to 0°, 4-(dimethylamino)pyridine (5 equiv.). The mixture was stirred for 2–5 d at r.t. and then quenched by the addition of sat. NaHCO₃ soln. The brown mixture was extracted with CH₂Cl₂, the org. phase washed with 10% citric acid, dried (Na₂SO₄ or MgSO₄), and evaporated. The resulting foam was dissolved in dioxane (0.04–0.07M), and 4-nitrophenol (1.4 equiv.) and DCC (2.8–4 equiv.) were added at r.t. After stirring for 1.5–16 h, filtration, and evaporation of the filtrate, residual polar solvents were removed by co-evaporation with toluene. The crude product was purified by CC and precipitation.

(3'*S*,5'*R*)-1-{2'-Deoxy-5'-O-[(4,4'-dimethoxytriphenyl)methyl]-3',5'-ethano-3'-O-[4-(4-nitrophenyloxy)succinyl]-β-D-ribofuranosyl}thymine (**16**). From **8** (150 mg, 0.263 mmol), succinic anhydride (263 mg, 2.628 mmol), 4-(dimethylamino)pyridine (160 mg, 1.310 mmol), pyridine (1.3 ml, 5 d), then 4-nitrophenol (51 mg, 0.368 mmol), DCC (206 mg, 0.998 mmol), and dioxane (4 ml, 1.5 h). CC (hexane/AcOEt 1:2) and precipitation (hexane) gave **16** (153 mg, 73%). Slightly brownish powder containing *ca.* 10% (¹H-NMR) of *N,N'*-dicyclohexylurea (DCU). TLC (hexane/AcOEt 1:4): R_f 0.59. ¹H-NMR (300 MHz, CDCl₃): 1.10–1.78 (*m*, H–C(6') and H–C(7')) (3 H, DCU); 1.79 (*d*, *J* = 1.1, Me–C(5)); 1.87 (*dd*, *J* = 9.0, 14.8, H–C(2'')); 2.04–2.11 (*m*, 1 H, H–C(6'), H–C(7'')); 2.66–2.70,

2.84–2.93 (2*m*, OCCH₂CH₂CO); 2.98 (*d*, *J* = 5.5, 14.7, 2 H–C(2'')); 3.79 (*s*, 2 MeO); 3.95–4.01 (*m*, H–C(4'), H–C(5'')); 6.18 (*dd*, *J* = 5.4, 8.9, H–C(1'')); 6.83 (*d*, *J* = 3.1, 4 arom. H); 7.20–7.31, 7.38–7.43, 7.49–7.53 (3*m*, 11 arom. H); 7.78 (*d*, *J* = 1.1, H–C(6)); 8.24–8.29 (*m*, 2 arom. H); 8.63 (*br. s*, NH). ¹³C-NMR (75 MHz, CDCl₃): 12.49 (*q*, Me–C(5)); 29.16, 29.36 (2*t*, OCCH₂CH₂CO); 30.78, 32.37, 34.15 (3*t*, C(6'), C(7'), DCU); 45.22 (*t*, C(2'')); 55.29 (*q*, MeO); 72.80 (*d*, C(5'')); 85.43, 86.27 (2*d*, C(1'), C(4'')); 87.34 (*s*, Ar₂CPh); 92.71 (*s*, C(3'')); 111.19 (*s*, C(5)); 113.27, 122.34, 125.29, 127.06, 127.97, 128.16, 130.17 (7*d*, arom. C); 135.15 (*d*, C(6)); 136.48, 136.58, 145.41 (3*s*, arom. C); 150.14 (*s*, C(2)); 155.25, 158.78 (2*s*, arom. C); 163.57 (*s*, C(4)); 169.96, 171.11 (2*s*, CO). FAB-MS (*pos.*): 791 (2, M⁺), 346 (20), 319 (15), 305 (22), 304 (78), 303 (100), 301 (11), 289 (20), 273 (13), 226 (11), 225 (38).

(3',5',5'R)-N⁶-Benzoyl-9-{2'-deoxy-5'-O-[(4,4'-dimethoxytriphenyl)methyl]-3',5'-ethano-3'-O-[4-(4-nitrophenyloxy)succinyl]-β-D-ribofuranosyl}adenine (17). From **9** (125 mg, 0.183 mmol) succinic anhydride (183 mg, 1.829 mmol), 4-(dimethylamino)pyridine (112 mg, 0.917 mmol), pyridine (1.0 ml, 2 d), then 4-nitrophenol (36 mg, 0.259 mmol), DCC (113 mg, 0.548 mmol), and dioxane (4 ml, 2 h). CC (AcOEt) and precipitation (hexane) gave **17** (104 mg, 63%). Slightly brownish powder. TLC (AcOEt): R_f 0.48. ¹H-NMR (400 MHz, CDCl₃): 1.51–1.71 (*m*, 3 H, H–C(6'), H–C(7'')); 2.09–2.14 (*dd*, *J* = 5.7, 13.0, 1 H, H–C(6'), H–C(7'')); 2.48 (*dd*, *J* = 8.4, 14.8, 1 H–C(2'')); 2.67–2.71, 2.87–2.90 (2*m*, 2 OCCH₂CH₂CO); 3.14 (*dd*, *J* = 5.8, 14.7, 1 H–C(2'')); 3.78 (*s*, 2 MeO); 3.91 (*d*, *J* = 5.4, H–C(4'')); 3.94–4.02 (*m*, H–C(5'')); 6.40 (*dd*, *J* = 5.8, 8.3, H–C(1'')); 6.80–6.84, 7.19–7.22, 7.26–7.30, 7.39–7.43, 7.50–7.56, 7.60–7.64 (6*m*, 18 arom. H); 8.04 (*d*, *J* = 7.2, 2 arom. H); 8.26 (*d*, *J* = 9.2, 2 arom. H); 8.49, 8.80 (2*s*, H–C(2'), H–C(8)); 9.08 (*br. s*, NH). ¹³C-NMR (100 MHz, CDCl₃): 29.16, 29.26 (2*t*, OCCH₂CH₂CO); 29.86, 33.03 (2*t*, C(6'), C(7'')); 46.58 (*t*, C(2'')); 55.25 (*q*, MeO); 73.20 (*d*, C(5'')); 85.10, 86.51 (2*d*, C(1'), C(4'')); 87.13 (*s*, Ar₂CPh); 92.23 (*s*, C(3'')); 113.22, 122.35 (2*d*, arom. C); 123.40 (*s*, C(5)); 125.26, 126.95, 127.90, 127.92, 128.91, 130.13, 130.17, 132.81 (8*d*, arom. C); 133.59, 136.64, 133.67 (3*s*, arom. C); 141.01 (*d*, C(8)); 145.40 (*s*, arom. C); 149.51 (*s*, C(4)); 151.41 (*s*, C(6)); 152.66 (*d*, C(2)); 155.20, 158.67 (2*s*, arom. C); 164.62, 170.00, 171.08 (3*s*, CO). FAB-MS (*pos.*): 905 (6.1, [M + 1]⁺), 304 (38), 303 (100), 240 (36), 225 (17).

(3',5',5'R)-N⁴-Benzoyl-1-{2'-deoxy-5'-O-[(4,4'-dimethoxytriphenyl)methyl]-3',5'-ethano-3'-O-[4-(4-nitrophenyloxy)succinyl]-β-D-ribofuranosyl}cytosine (18). From **10** (240 mg, 0.36 mmol), succinic anhydride (364 mg, 3.6 mmol), 4-(dimethylamino)pyridine (220 mg, 1.8 mmol), pyridine (2.0 ml, 67 h), then 4-nitrophenol (71 mg, 0.51 mmol), DCC (210 mg, 1.02 mmol), and dioxane containing 15% (*v/v*) pyridine (1.1 ml, 4 h). CC (CH₂Cl₂/MeOH 20:1) and repeated precipitation (hexane) gave **18** (235 mg, 73%). Slightly brownish powder. TLC (CH₂Cl₂/MeOH 20:1): R_f 0.54. ¹H-NMR (400 MHz, CDCl₃): 1.43–1.58, 2.03–2.06 (2*m*, H–C(6'), H–C(7'')); 1.88 (*dd*, *J* = 8.0, 15.2, 1 H–C(2'')); 2.66 (*t*, *J* = 6.8, 2 H, OCCH₂CH₂CO); 2.79–2.93 (*m*, 2 H, OCCH₂CH₂CO); 3.31 (*dd*, *J* = 5.9, 15.2, 1 H–C(2'')); 3.80 (*s*, 2 MeO); 3.89 (*d*, *J* = 6.1, H–C(4'')); 3.97–4.03 (*m*, H–C(5'')); 6.14 (*dd*, *J* = 5.9, 7.8, H–C(1'')); 6.85–6.87, 7.23–7.25, 7.27–7.34, 7.40–7.45, 7.51–7.55, 7.61–7.65, 8.21–8.30 (7*m*, 21 H, arom. H, H–C(5)); 7.90 (*d*, *J* = 7.3, 2 arom. H); 8.72 (*d*, *J* = 7.5, H–C(6)). ¹³C-NMR (100 MHz, CDCl₃): 29.1, 29.3 (2*t*, OCCH₂CH₂CO); 30.4, 32.2 (2*t*, C(6'), C(7'')); 47.1 (*t*, C(2'')); 55.3 (*q*, MeO); 72.9 (*d*, C(5'')); 86.8, 87.9 (2*d*, C(1'), C(4'')); 87.6 (*s*, Ar₂CPh); 92.9 (*s*, C(3'')); 96.6 (*d*, C(5)); 113.3, 122.4, 125.3, 127.1, 127.5, 128.0, 128.1, 129.1, 130.15, 130.20, 133.2 (11*d*, arom. C); 133.1, 136.41, 136.44, 145.3, 145.5, 155.2, 158.8 (7*s*, arom. C); 144.8 (*d*, C(6)); 154.9 (*s*, C(2)); 162.3 (*s*, C(4)); 166.5, 169.9, 171.0 (3*s*, CO). FAB-MS (*pos.*): 881 (1.5, M⁺), 399 (1), 304 (28), 303 (100), 216 (12).

(3',5',5'R)-9-{2'-Deoxy-5'-O-[(4,4'-dimethoxytriphenyl)methyl]-3',5'-ethano-3'-O-[4-(4-nitrophenyloxy)succinyl]-β-D-ribofuranosyl}-N²-isobutyrylguanine (19). From **11** (132 mg, 0.198 mmol), succinic anhydride (198 mg, 1.98 mmol), 4-(dimethylamino)pyridine (121 mg, 0.99 mmol), pyridine (1.0 ml, 48 h), then 4-nitrophenol (35 mg, 0.25 mmol), DCC (103 mg, 0.497 mmol), and dioxane/CH₂Cl₂ 2:1 containing 10% (*v/v*) pyridine (1.6 ml, 16 h). CC (AOEt) gave **19** (108 mg, 68%). Slightly yellowish foam. Anal. data were obtained from a sample (21 mg) that was precipitated from hexane (17 mg, white powder). TLC (CH₂Cl₂/MeOH 20:1): R_f 0.62. ¹H-NMR (400 MHz, CDCl₃): 1.23–1.26 (*m*, Me₂CH); 1.49–1.61, 2.02–2.09 (2*m*, 2 H–C(6'), 2 H–C(7'')); 2.33 (*dd*, *J* = 8.3, 14.8, 1 H–C(2'')); 2.52–2.63 (*m*, Me₂CH); 2.64–2.67, 2.84–2.88 (2*m*, OCCH₂CH₂CO); 3.00 (*dd*, *J* = 5.9, 14.8, 1 H–C(2'')); 3.77, 3.78 (2*s*, 2 MeO); 3.87 (*d*, *J* = 5.8, H–C(4'')); 3.91–3.97 (*m*, H–C(5'')); 6.09 (*dd*, *J* = 5.9, 8.2, H–C(1'')); 7.18–7.23, 7.24–7.28, 7.37–7.41, 7.48–7.52 (4*m*, 9 arom. H); 8.13 (*s*, H–C(8)); 8.23–8.27 (*m*, 2 arom. H); 8.38, 12.00 (2 *br. s*, NH). ¹³C-NMR (100 MHz, CDCl₃): 19.0 (*q*, Me₂CH); 29.1, 29.2 (2*t*, OCCH₂CH₂CO); 29.8, 33.2 (2*t*, Ar₂CPh); 36.6 (*d*, Me₂CH); 46.7 (*t*, C(2'')); 55.3 (*q*, MeO); 73.2 (*d*, C(5'')); 84.8, 86.4 (2*d*, C(1'), C(4'')); 87.1 (*s*, C(6'), C(7'')); 113.2, 122.3, 125.3, 127.0, 127.9, 128.2, 130.1, 130.2 (8*d*, arom. C); 136.1 (*d*, C(8)); 136.67, 136.69 (2*s*, arom. C); 145.4, 145.5, 147.3, 147.5 (4*s*, C(4), C(2), arom. C); 155.2, 155.5 (2*s*, C(6), arom. C); 158.67, 158.69 (2*s*, arom. C); 170.2, 171.1, 178.1 (3*s*, CO). FAB-MS (*pos.*): 887 (0.6, [M + 1]⁺), 886 (0.1, M⁺), 304 (25), 303 (100), 222 (8).

Nucleoside-Modified Solid Support: General Procedure. To a soln. of the activated esters **16–19** in dioxane/DMF/Et₃N 1:2:0.2 (0.06*M*) was added long-chain-alkylamine-CPG (0.5 g/0.1 mmol **16–19**) and the resulting

suspension slowly stirred for 24–48 h. After filtration and extensive washing with DMF, MeOH, and Et₂O, the solid support was dried (high vacuum) and the loading capacity determined by the trityl assay [10]. Unreacted amino groups on the solid support were capped by treatment with pyridine/Ac₂O 5:0.5 containing 4-(dimethylamino)pyridine (5 mol-% rel. to Ac₂O) (5.5 ml soln./0.5 g CPG). Repeated preparations of solid support (scale: 0.5–1.1 g CPG) led to loading capacities ranging from 22–39 μmol/g.

Oligo(bicyclodeoxynucleotides). The synthesis of oligonucleotides was performed on a *Pharmacia Gene Assembler Special* connected to a *Compaq-ProLinea-3/25-zs* personal computer. For syntheses below the 1.5-μmol level, the 1.3-μmol cycle, and above the 1.5-μmol level, the 10-μmol synthetic cycle was used. Reagent soln. were prepared according to the manufacturers protocol [13] with the exception of dry MeCN that was bought from *Rathburn*. Phosphoramidite (0.1M) and 1*H*-tetrazole (0.5M) soln. were equal in concentration to those used for the synthesis of natural oligodeoxynucleotides. Synthesis conditions are given in *Scheme 2*. Coupling efficiencies as monitored by on-line trityl assay were generally higher than 98%. The last step in every synthesis was the removal of the 5'-protecting group (trityl-off mode). After synthesis, the solid support was suspended in conc. NH₃ soln. and left for 10–16 h at 55° to effect deprotection. Evaporation, redissolution in H₂O, followed by filtration yielded the crude oligonucleotide soln. that was subsequently used for HPLC purification (*Table 6*). All natural oligodeoxynucleotides that were used for comparison of biophysical properties were synthesized according to the standard procedure and purified by HPLC. UV-Spectroscopically determined yields after chromatographic purification were in the range of 16–41% (*Table 6*).

Table 6. *Synthesis and Chromatography Data of Oligodeoxynucleotides*

Sequence	Scale [μmol]	HPLC	OD (260 nm) (yield [%])
bcd(T ₁₀)	1.3	DEAE ^a): 20–50% <i>B</i> in 40 min; <i>t_R</i> 19 min reversed-phase ^b): 15–16% <i>B</i> in 20 min; <i>t_R</i> 14 min	42.0 (38)
bcd(A ₁₀)	10.2	DEAE ^c): 40–75% <i>B</i> in 30 min; <i>t_R</i> 23 min reversed-phase ^d): 15–22% <i>B</i> in 30 min; <i>t_R</i> 18 min	297.3 (28)
(bcdT-dT) ₅	0.9	DEAE ^a): 20–50% <i>B</i> in 40 min; <i>t_R</i> 26 min reversed-phase ^b): 15–22% <i>B</i> in 30 min; <i>t_R</i> 15 min	20.8 (25)
d(A ₁₀)	1.32	DEAE ^a): 40–75% <i>B</i> in 30 min; <i>t_R</i> 26 min reversed-phase ^d): 13–19% <i>B</i> in 30 min; <i>t_R</i> 15 min	42.2 (30)
d(T ₁₀)	10.0	DEAE ^c): 25–65% <i>B</i> in 30 min; <i>t_R</i> 15 min reversed-phase ^b): 15–22% <i>B</i> in 30 min; <i>t_R</i> 17 min	337.2 (35)
d(T ₅ -A-T ₄)	1.3	DEAE ^c): 25–65% <i>B</i> in 30 min; <i>t_R</i> 17 min reversed-phase ^b): 15–22% <i>B</i> in 30 min; <i>t_R</i> 14 min	51.2 (41)
d(T ₅ -C-T ₄)	1.0	DEAE ^c): 25–65% <i>B</i> in 30 min; <i>t_R</i> 18 min reversed-phase ^b): 15–22% <i>B</i> in 30 min; <i>t_R</i> 14 min	33.6 (36)
d(T ₅ -G-T ₄)	1.3	DEAE ^c): 25–65% <i>B</i> in 30 min; <i>t_R</i> 17 min reversed-phase ^b): 15–22% <i>B</i> in 30 min; <i>t_R</i> 12 min	48.1 (38)

^a) *Nucleogen DEAE 60-7*, 125 × 4.0 mm (*Macherey & Nagel*); *A*: 20 mM KH₂PO₄ in H₂O/MeCN 4:1, pH 6.0; *B*: *A* + 1M KCl; flow: 1 ml/min; detection: 260 nm.

^b) *Aquapore Rp-300*, 220 × 4.6 mm, 7 μm (*Brownlee Labs*); *A*: 0.1M (Et₃NH)OAc in H₂O, pH 7.0; *B*: 0.1M (Et₃NH)OAc in H₂O/MeCN 1:4, pH 7.0; flow: 1 ml/min; detection: 260 nm.

^c) *Nucleogen DEAE 60-7*, 125 × 10.0 mm (*Macherey & Nagel*); *A*: 20 mM KH₂PO₄ in H₂O/MeCN 4:1, pH 6.0; *B*: *A* + 1M KCl; flow: 3 ml/min; detection: 260 nm.

^d) *Spherisorb-SIOX RP-C18*, 10 μm, 300 Å, 220 × 12 mm; *A*: 0.1M (Et₃NH)OAc in H₂O, pH 7.0; *B*: 0.1M (Et₃NH)OAc in H₂O/MeCN 1:4, pH 7.0; flow: 4 ml/min; detection: 260 nm.

Enzymatic Degradation of Oligonucleotides. Ca. 1 ml of a ca. 4 μM soln. of the oligomer in 10 mM Tris · HCl/0.15M NaCl (pH 7.0) was incubated at 37° with 2 μl of a soln. of phosphodiesterase from *Crotalus durissus* (2 mg/ml) and 5 μl of a soln. of alkaline phosphatase from calf intestine (1 mg/ml). After 24 h, an aliquot of this soln. was directly subjected to HPLC analysis.

REFERENCES

- [1] M. Tarköy, C. Leumann, *Angew. Chem.* **1993**, *105*, 1516; *ibid. Int. Ed.* **1993**, *32*, 1432.
- [2] M. Tarköy, 'Nukleinsäure-Analoga mit konformationell eingeschränktem Zucker-Phosphat-Rückgrat (Bicyclo-DNS): Synthese und Eigenschaften adenin- und thyminhaltiger Bicycloooligonukleotide', Diss. No. 10109, ETH Zürich, 1993.
- [3] M. Bolli, 'Nukleinsäure-Analoga mit konformationell eingeschränktem Zucker-Phosphat-Rückgrat (Bicyclo-DNS): Synthese und Eigenschaften gemischtbasiger Bicycloooligonukleotide', Diss. University of Bern, in preparation.
- [4] E. Uhlmann, A. Peyman, *Chem. Rev.* **1990**, *90*, 543–584; J. Goodchild, *Bioconjugate Chem.* **1990**, *1*, 165; U. Englisch, D. Gauss, *Angew. Chem.* **1991**, *103*, 629; *ibid. Int. Ed.* **1991**, *30*, 613.
- [5] M. Tarköy, M. Bolli, B. Schweizer, C. Leumann, *Helv. Chim. Acta* **1993**, *76*, 481.
- [6] M. Egli, P. Lubini, M. Bolli, M. Dobler, C. Leumann, *J. Am. Chem. Soc.* **1993**, *115*, 5855.
- [7] M. D. Matteucci, M. H. Caruthers, *J. Am. Chem. Soc.* **1981**, *103*, 3185; S. L. Beaucage, M. H. Caruthers, *Tetrahedron Lett.* **1981**, *22*, 1859; L. J. McBride, M. H. Caruthers, *ibid.* **1983**, *24*, 245; S. P. Adams, K. S. Kavka, E. J. Wykes, S. B. Holder, G. R. Galluppi, *J. Am. Chem. Soc.* **1983**, *105*, 661; N. D. Sinha, J. Biernat, H. Köster, *Tetrahedron Lett.* **1983**, *24*, 5843; N. D. Sinha, J. Biernat, J. McManus, H. Köster, *Nucleic Acids Res.* **1984**, *12*, 4539.
- [8] R. L. Letsinger, J. L. Finnan, G. A. Heavner, W. B. Lunsford, *J. Am. Chem. Soc.* **1975**, *97*, 3278; R. L. Letsinger, W. B. Lunsford, *ibid.* **1976**, *98*, 3655.
- [9] M. H. Caruthers, *Acc. Chem. Res.* **1991**, *24*, 278.
- [10] A. R. Jones, in 'Oligonucleotide Synthesis – a Practical Approach', Ed. M. J. Gait, IRL Press, Oxford, 1984, p. 23ff.
- [11] M. P. Reddy, J. B. Rampil, S. L. Beaucage, *Tetrahedron Lett.* **1987**, *28*, 23.
- [12] IUPAC-IUB, 'Abbreviations and Symbols for the Description of Conformations of Polynucleotide Chains', *Pure Appl. Chem.* **1983**, *55*, 1273.
- [13] 'Gene Assembler® Special, Users Manual, Vers. 1.51', *Pharmacia LKB Biotechnology AB*, Uppsala.
- [14] U. Pieleles, W. Zücher, M. Schär, H. E. Moser, *Nucleic Acids Res.* **1993**, *21*, 3139.
- [15] P. Job, *Anal. Chim. Acta* **1928**, *9*, 113.
- [16] M. Riley, B. Maling, M. J. Chamberlin, *J. Mol. Biol.* **1966**, *20*, 359.
- [17] a) S. B. Zimmerman, B. H. Pfeiffer, *Proc. Natl. Acad. Sci. U. S. A.* **1981**, *78*, 78; b) J. M. Benevides, G. J. Thomas, Jr., *Biochemistry* **1988**, *27*, 3868.
- [18] a) S. Arnott, R. Chandrasekaran, R. P. Millane, H.-S. Park, *J. Mol. Biol.* **1986**, *188*, 631; b) H. T. Steely, Jr., D. M. Gray, R. L. Ratliff, *Nucleic Acids Res.* **1986**, *14*, 10071.
- [19] S.-H. Chou, P. Flynn, B. Reid, *Biochemistry* **1989**, *28*, 2435.
- [20] R. F. Macaya, P. Schultze, J. Feigon, *J. Am. Chem. Soc.* **1992**, *114*, 781; R. F. Macaya, E. Wang, P. Schultze, J. Feigon, *J. Mol. Biol.* **1992**, *225*, 755.
- [21] R. W. Roberts, D. M. Crothers, *Science* **1992**, *258*, 1463; H. Han, P. B. Dervan, *Proc. Natl. Acad. Sci. U. S. A.* **1993**, *90*, 3806; C. Escudé; J.-C. François, J.-S. Sun, G. Ott, M. Sprinzl, T. Garestier, C. Hélène, *Nucleic Acids Res.* **1993**, *21*, 5547.
- [22] D. S. Pilch, C. Levenson, R. H. Shafer, *Proc. Natl. Acad. Sci. U. S. A.* **1990**, *87*, 1942.
- [23] M. T. Record Jr., C. F. Anderson, T. M. Lohman, *Q. Rev. Biophys.* **1978**, *11*, 103; G. S. Manning, *ibid.* **1978**, *11*, 179.
- [24] C. R. Cantor, P. R. Schimmel, 'Biophysical Chemistry Part III: The Behavior of Biological Macromolecules', W. H. Freeman & Co., New York, 1980.
- [25] a) K. J. Breslauer, in 'Thermodynamic Data for Biochemistry and Biotechnology', Ed. H.-J. Hinz, Springer-Verlag, Berlin, 1986, Chapt. 15; b) L. A. Marky, K. J. Breslauer, *Biopolymers* **1986**, *26*, 1601.
- [26] a) G. E. Plum, Y.-W. Park, S. F. Singleton, P. B. Dervan, K. J. Breslauer, *Proc. Natl. Acad. Sci. U. S. A.* **1990**, *87*, 9436; b) J. Völker, D. P. Botes, G. G. Lindsey, H. H. Klump, *J. Mol. Biol.* **1993**, *230*, 1278.
- [27] R. Jin, W. H. Chapman, Jr., A. R. Srinivasan, W. K. Olson, R. Breslow, R. J. Breslauer, *Proc. Natl. Acad. Sci. U. S. A.* **1993**, *90*, 10568.
- [28] J. M. Sturtevant, *Methods Enzymol.* **1972**, *26*, 227; R. L. Biltonen, N. Langerman, *ibid.* **1979**, *61*, 287.
- [29] T. Wiseman, S. Williston, J. F. Brandts, L.-N. Lin, *Anal. Biochem.* **1989**, *179*, 131.
- [30] G. Vesnaver, K. J. Breslauer, *Proc. Natl. Acad. Sci. U. S. A.* **1991**, *88*, 3569.
- [31] L. E. Xodo, G. Manzini, F. Quadrifoglio, *Nucleic Acids Res.* **1990**, *18*, 3557; G. Manzini, L. E. Xodo, D. Gasparotto, F. Quadrifoglio, G. A. van der Marel, J. H. van Boom, *J. Mol. Biol.* **1990**, *213*, 833; C.

- Giovannangeli, T. Montenay-Garestier, M. Rougée, M. Chassignol, N. T. Thuong, C. Hélène, *J. Am. Chem. Soc.* **1991**, *113*, 7775.
- [32] G. Prakash, E. T. Kool, *J. Chem. Soc., Chem. Commun.* **1991**, 1161; E. T. Kool, *J. Am. Chem. Soc.* **1991**, *113*, 6265; D. J. D'Souza, E. T. Kool, *J. Biomol. Struct. Dyn.* **1992**, *10*, 141.
- [33] R. J. Jones, S. Swaminathan, J. F. Milligan, S. Wadwani, B. C. Froehler, M. D. Matteucci, *J. Am. Chem. Soc.* **1993**, *115*, 9816.
- [34] S. Fujimori, K. Shudo, *J. Am. Chem. Soc.* **1990**, *112*, 7436.
- [35] B. Meng, S. H. Kawai, D. Wang, G. Just, P. A. Giannaris, M. J. Damha, *Angew. Chem.* **1993**, *105*, 733; *ibid. Int. Ed.* **1993**, *32*, 729.
- [36] W. Saenger, 'Principles of Nucleic Acid Structure', Springer Advanced Texts in Chemistry, Ed. C. R. Cantor, Springer Verlag, New York, 1984, Chapt. 2, p. 9–28.
- [37] P. Lubini, M. Egli, 'Proceedings of the 8th Conversation in Biomolecular Stereodynamics', Eds. R. H. Sarma and M. H. Sarma, Adenine Press, New York, 1994, in press.
- [38] R. E. Dickerson, H. R. Drew, *J. Mol. Biol.* **1981**, *149*, 761.
- [39] J. Hunziker, H.-J. Roth, M. Böhringer, A. Giger, U. Diederichsen, M. Göbel, R. Krishnan, B. Jaun, C. Leumann, A. Eschenmoser, *Helv. Chim. Acta* **1993**, *76*, 259.
- [40] S. Pitsch, S. Wendeborn, B. Jaun, A. Eschenmoser, *Helv. Chim. Acta* **1993**, *76*, 2161.
- [41] J. S. Eadie, L. J. McBride, J. W. Efcavitch, L. B. Hoff, R. Cathcraft, *Anal. Biochem.* **1987**, *165*, 442.